



The chlorite proximator: A new tool for detecting porphyry ore deposits



Jamie J. Wilkinson^{a,b,*}, Zhaoshan Chang^{a,1}, David R. Cooke^a, Michael J. Baker^a, Clara C. Wilkinson^{a,2}, Shaun Inglis^a, Huayong Chen^{a,3}, J. Bruce Gemmell^a

^a ARC Centre of Excellence in Ore Deposit Research (CODES), University of Tasmania, Private Bag 79, Hobart, Tasmania 7001, Australia

^b Department of Earth Science and Engineering, Imperial College London, Exhibition Road, London SW7 2AZ, United Kingdom

ARTICLE INFO

Article history:

Received 21 August 2014

Accepted 19 January 2015

Available online 28 January 2015

Keywords:

Chlorite
Chemistry
Propylitic
Porphyry
Exploration
Geothermometry

ABSTRACT

The major, minor and trace element chemistry of chlorite were evaluated as a tool for mineral exploration in the propylitic environment of porphyry ore deposits. Chlorite from eighty propylitically altered samples, located up to 5 km from the Batu Hijau Cu–Au porphyry deposit in Indonesia, was analyzed using electron microprobe and laser ablation inductively-coupled plasma mass spectrometry. The results show that a variety of elements, including K, Li, Mg, Ca, Sr, Ba, Ti, V, Mn, Co, Ni, Zn and Pb, are probably incorporated in the chlorite lattice and display systematic spatial variations relative to the porphyry center. Ti, V and Mg decrease exponentially in concentration with increasing distance, whereas the others increase. Ratioing the former to the latter provides a variety of ratios that vary up to four orders of magnitude, providing sensitive vectoring parameters. Chlorite geothermometry suggests that Ti is substituted into chlorite as a function of crystallization temperature and thus maps out the thermal anomaly associated with the mineralized center. By contrast, Mn and Zn display a maximum in chlorite at a distance of ~1.3 km that mirrors the whole rock anomaly for these metals, reflecting their lateral advection into the wall rocks by magmatic-hydrothermal fluids. The recognizable footprint defined by chlorite compositions extends to at least 4.5 km, significantly beyond the whole rock anomalism (≤ 1.5 km) and thus represents a powerful new exploration tool for detecting porphyry systems. Variations in chlorite chemistry are very systematic in the inner propylitic zone (to distances of ~2.5 km), thereby providing a precise vectoring tool in a domain where other tools are typically ineffective. In this zone, equations of the form:

$$x = \frac{\ln \left\{ \frac{R}{a} \right\}}{b}$$

can be formulated, where the distance to center, x , is predicted based on a variety of element ratios in chlorite R , and where a and b are exponential fit parameters. Importantly, distal chlorite compositions in porphyry-related propylitic alteration systems are also shown to be distinct from metamorphic chlorite, allowing the external fringes of porphyry-related hydrothermal systems to be distinguished from “background” regional metamorphism or geothermal alteration.

Crown Copyright © 2015 Published by Elsevier B.V. This is an open access article under the CC BY-NC-ND license (<http://creativecommons.org/licenses/by-nc-nd/4.0/>).

1. Introduction

Porphyry ore deposits represent remarkable accumulations of metals, in particular Cu, Mo and Au, which are precipitated from hydrothermal fluids in an intrusive host and surrounding country rocks.

Deposits are typically centered within an alteration halo that displays characteristic mineralogical and chemical zoning patterns (Lowell & Guilbert, 1970). This footprint is a key guide for exploration, providing a larger (up to 10 km radius) target area within which mineralization may exist. However, the mineral assemblages that characterize these alteration zones may be present within barren hydrothermal systems, or produced by processes such as regional metamorphism. Discriminating mineralized and barren environments, locating hydrothermal centers within or beneath a zone of altered rocks, and recognizing the fringes of ore systems continue to be great challenges to the exploration industry. From a scientific standpoint, the controls on the formation of these huge alteration zones are incompletely understood.

Here, we present microprobe and laser ablation inductively-coupled plasma mass spectrometry (LA-ICP-MS) analyses of chlorite from the

* Corresponding author at: Department of Earth Sciences, Natural History Museum, Cromwell Road, London SW7 5BD, United Kingdom. Tel.: +44 20 79425334.

E-mail address: j.wilkinson@nhm.ac.uk (J.J. Wilkinson).

¹ Current address: School of Earth and Environmental Sciences, Building 34, James Cook University, Townsville, QLD 4811, Australia.

² Current address: Department of Earth Sciences, Natural History Museum, Cromwell Road, London SW7 5BD, United Kingdom.

³ Current address: Guangzhou Institute of Geochemistry, Chinese Academy of Sciences, 511 Kehua Street, Tianhe, PO Box 1131, Guangzhou, China, 510640.

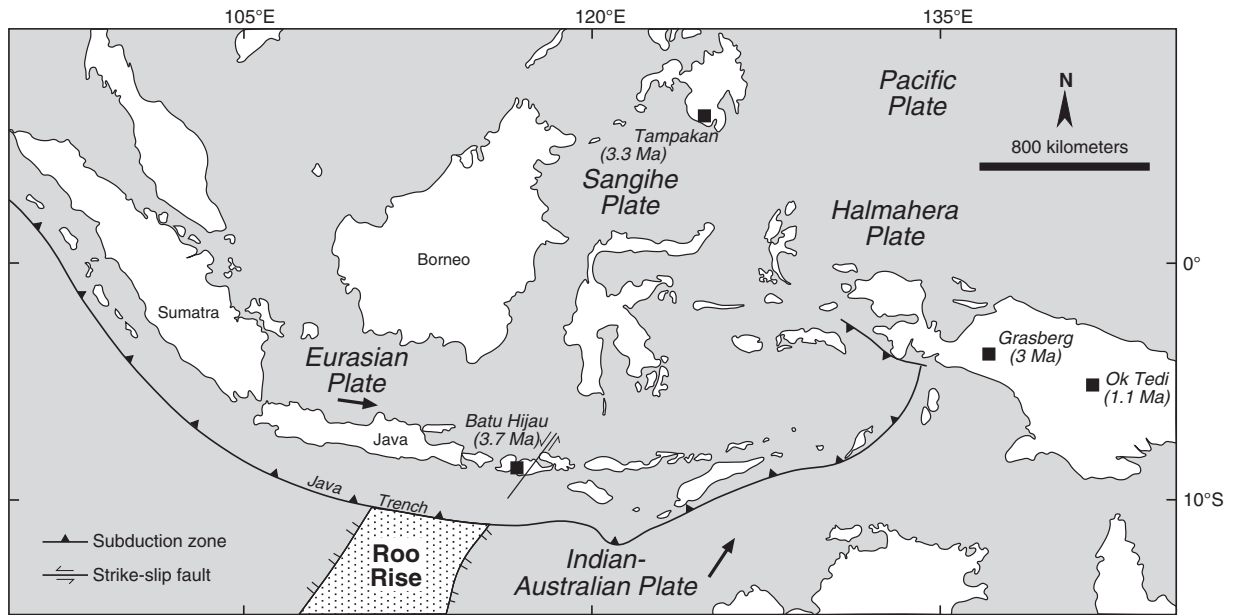


Fig. 1. Map showing the location of Batu Hijau on Sumbawa Island, Indonesia, north of the Java Trench.

propylitic alteration halo of the giant Batu Hijau porphyry copper–gold deposit in Indonesia. The results represent a breakthrough for exploration because they show that the chemistry of chlorite, one of the most common alteration minerals in hydrothermal systems, varies systematically and can be used as a tool to determine the direction towards, and estimate the distance from, mineralized intrusions. Chlorite geothermometry suggests that some trace elements (e.g., Ti) may be controlled by crystallization temperature, reflecting conduction and advection of heat away from a magmatic-hydrothermal center. Anomalous concentrations of metals that are typically enriched in porphyry magmatic-hydrothermal fluids indicate either that fluxes of

magmatic fluids influence a much larger volume of rock than previously thought, or extensive outward remobilization or dispersion of magmatic metals occurs via circulating formation waters at elevated temperature. Chlorite compositions from the distal fringes of the porphyry system are also distinct from metamorphic chlorites, providing a practical environmental discriminator.

2. The green rock environment

The ‘green rock’ environment of propylitic alteration, in which hydrothermal minerals such as actinolite, albite, epidote, calcite

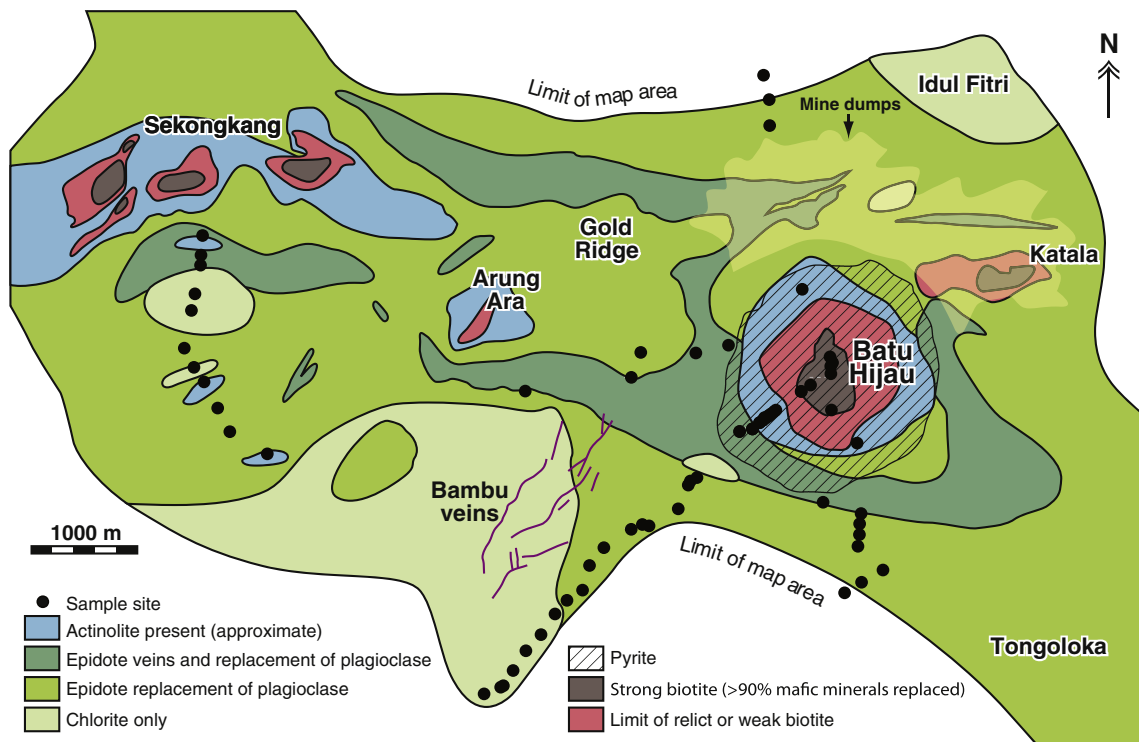


Fig. 2. Early stage alteration map of the Batu Hijau district (modified after Garwin, 2000) showing sample locations.

Table 1

All concentrations reported in parts per million (ppm).

Sample	Easting	Northing	Elevation (m)	Distance to center (m)	Mean temperature ^s (°C)	Ag	Al	As	Au	B	Ba	Bi	Ca	Ce	Co	Cr	Cu	Eu	Fe	Ga	Hf	K	La	Li	Lu	Mg
BH04_52	484293	9008004	720	1565	148	n.d.	88707	n.d.	n.d.	n.d.	0.6	n.d.	2862	0.015	n.d.	n.d.	22.5	n.d.	144459	42	n.d.	82	0.014	n.d.	0.018	150851
BH04_53	484228	9007970	750	1637	176	n.d.	100344	0.44	0.023	n.d.	2.2	0.006	2986	0.221	n.d.	n.d.	281.5	0.026	147004	38	0.009	42	0.146	n.d.	0.011	156144
BH04_54	484207	9007930	774	1678	157	n.d.	104028	0.26	n.d.	n.d.	1.4	0.019	3547	0.072	n.d.	n.d.	192.8	0.027	134653	38	0.028	68	0.027	n.d.	n.d.	138984
BH04_55B	484108	9007694	870	1909	200	n.d.	98801	0.61	n.d.	n.d.	14.5	0.016	8065	0.055	n.d.	n.d.	50.0	0.007	123030	35	0.011	251	0.015	n.d.	0.010	142582
BH10-101	483820	9007524	879	2236	220	n.d.	99792	0.59	n.d.	5.5	2.7	n.d.	1316	0.009	154	2.6	70.5	n.d.	116177	51	n.d.	588	1.187	31	n.d.	146578
BH10-102	483754	9007538	875	2277	162	n.d.	90876	0.73	n.d.	3.7	10.2	n.d.	1872	0.027	138	5.1	189.3	n.d.	133214	44	n.d.	482	0.029	40	n.d.	149017
BH10-103	483644	9007490	849	2393	144	n.d.	88340	1.18	n.d.	4.4	14.5	n.d.	3910	0.092	116	112.6	98.6	n.d.	142352	31	n.d.	141	0.045	22	n.d.	141023
BH10-104	483374	9007308	805	2717	125	n.d.	105427	2.57	n.d.	11.4	11.2	n.d.	4945	0.222	124	17.7	66.3	n.d.	85876	66	n.d.	645	9.137	68	n.d.	140103
BH10-105	483232	9007131	795	2939	130	0.100	95414	2.02	n.d.	9.5	3.2	n.d.	2960	0.234	130	21.8	98.8	n.d.	103668	53	n.d.	790	0.757	30	n.d.	141980
BH10-106	483163	9006886	823	3151	143	n.d.	91730	3.14	n.d.	11.4	5.8	0.108	4939	1.195	130	39.2	140.4	n.d.	92381	48	n.d.	1027	0.581	35	n.d.	127519
BH10-107	483009	9006784	776	3334	158	n.d.	111774	2.22	n.d.	6.7	28.5	n.d.	2935	0.043	123	15.0	67.1	n.d.	104910	62	n.d.	169	0.029	55	n.d.	126285
BH10-108	482891	9006649	778	3512	113	n.d.	92623	1.22	n.d.	5.5	26.8	n.d.	6235	0.106	157	10.8	89.5	n.d.	106890	48	n.d.	535	0.036	54	n.d.	149210
BH10-109	482753	9006444	769	3752	117	0.047	87250	1.50	n.d.	14.4	32.2	n.d.	4151	0.176	136	22.7	227.2	n.d.	108110	49	n.d.	1287	0.709	34	n.d.	132503
BH10-110	482604	9006283	734	3971	105	n.d.	84738	1.01	n.d.	4.3	34.1	0.017	5302	0.108	145	6.5	123.0	n.d.	108641	39	n.d.	883	0.210	33	n.d.	163107
BH10-111	482477	9006087	716	4198	43	n.d.	80468	2.54	n.d.	6.3	17.8	0.021	9127	0.033	189	2.1	1135.8	n.d.	79251	39	n.d.	1434	0.888	26	n.d.	137193
BH10-112	482381	9005936	706	4372	51	0.029	78915	0.51	n.d.	7.7	3.3	0.012	10269	0.416	228	60.6	60.6	n.d.	52960	32	n.d.	641	0.187	34	n.d.	189023
BH10-113	482355	9005921	696	4401	81	n.d.	80546	1.42	n.d.	4.5	11.4	n.d.	9055	0.046	119	2.5	70.5	n.d.	117247	44	n.d.	707	0.025	32	n.d.	157799
BH10-114	482191	9005855	682	4565	77	n.d.	82213	0.68	n.d.	9.9	50.1	0.022	7541	0.461	242	28.6	71.2	n.d.	107672	40	n.d.	1496	0.539	32	n.d.	150627
BH10-115	481993	9005778	641	4762	n.c.	0.053	60850	5.83	n.d.	10.8	17.1	0.014	11529	5.099	243	5.6	36.8	n.d.	172741	33	n.d.	793	1.752	22	n.d.	91835
BH-17	481689	9008370	187	3863	n.c.	n.a.	n.a.	n.a.	n.a.	n.a.	n.a.	n.a.	n.a.	n.a.	n.a.	n.a.	n.a.	n.a.	n.a.	n.a.	n.a.	n.a.	n.a.	n.a.	n.a.	n.a.
BH-18	482557	9008826	260	2948	n.c.	n.a.	n.a.	n.a.	n.a.	n.a.	n.a.	n.a.	n.a.	n.a.	n.a.	n.a.	n.a.	n.a.	n.a.	n.a.	n.a.	n.a.	n.a.	n.a.	n.a.	n.a.
BH-19	482597	9008864	270	2906	n.c.	n.d.	106909	1.77	n.d.	n.d.	3.0	0.006	1460	0.058	n.d.	n.d.	3.0	0.014	156833	39	0.026	30	0.029	n.d.	0.018	145927
BH-20	483322	9009144	315	2183	n.c.	n.a.	n.a.	n.a.	n.a.	n.a.	n.a.	n.a.	n.a.	n.a.	n.a.	n.a.	n.a.	n.a.	n.a.	n.a.	n.a.	n.a.	n.a.	n.a.	n.a.	n.a.
BH-21	483645	9009000	330	1855	n.c.	n.d.	106775	0.48	n.d.	n.d.	3.8	0.013	433	0.017	n.d.	n.d.	79.8	0.006	151587	28	0.012	22	0.009	n.d.	0.007	160927
BH-22	483738	9009248	350	1779	n.c.	n.d.	100419	0.22	n.d.	n.d.	1.6	n.d.	256	n.d.	n.d.	n.d.	0.8	n.d.	155935	51	n.d.	15	n.d.	n.d.	n.d.	160569
BH-23	483817	9009356	340	1720	n.c.	n.a.	n.a.	n.a.	n.a.	n.a.	n.a.	n.a.	n.a.	n.a.	n.a.	n.a.	n.a.	n.a.	n.a.	n.a.	n.a.	n.a.	n.a.	n.a.	n.a.	n.a.
BH-24	484282	9009242	350	1242	247	n.d.	98321	0.74	n.d.	n.d.	2.7	n.d.	727	0.038	n.d.	n.d.	5.3	0.037	152237	30	0.058	25	n.d.	n.d.	0.014	157113
BH-25	484605	9009320	350	950	335	n.d.	112680	0.50	n.d.	n.d.	3.0	0.154	385	0.050	n.d.	n.d.	1.2	0.007	129123	44	n.d.	51	0.026	n.d.	0.008	170666
BH-26	484665	9009140	360	847	n.c.	n.a.	n.a.	n.a.	n.a.	n.a.	n.a.	n.a.	n.a.	n.a.	n.a.	n.a.	n.a.	n.a.	n.a.	n.a.	n.a.	n.a.	n.a.	n.a.	n.a.	n.a.
BH-27	484785	9008815	370	739	n.c.	n.a.	n.a.	n.a.	n.a.	n.a.	n.a.	n.a.	n.a.	n.a.	n.a.	n.a.	n.a.	n.a.	n.a.	n.a.	n.a.	n.a.	n.a.	n.a.	n.a.	n.a.
BH-35	483243	9010000	140	2469	n.c.	n.a.	n.a.	n.a.	n.a.	n.a.	n.a.	n.a.	n.a.	n.a.	n.a.	n.a.	n.a.	n.a.	n.a.	n.a.	n.a.	n.a.	n.a.	n.a.	n.a.	n.a.
Ep-01	485539	9007759	300	1304	263	n.d.	103600	0.89	n.d.	18.8	3.1	n.d.	732	0.007	119	n.d.	7.1	n.d.	164281	n.d.	n.d.	29	0.007	29	n.d.	158017
Ep-02	485914	9007647	300	1470	219	0.034	105889	0.17	n.d.	n.d.	1.7	n.d.	977	0.002	87	n.d.	10.8	n.d.	194019	n.d.	n.d.	80	n.d.	31	n.d.	129544
Ep-03	485900	9007545	300	1561	223	n.d.	104750	1.06	n.d.	4.4	1.2	n.d.	1603	0.473	77	n.d.	21.7	n.d.	147355	n.d.	n.d.	258	0.223	32	n.d.	80541
Ep-04	485898	9007438	300	1661	178	0.055	96467	2.00	n.d.	3.8	3.7	n.d.	2320	0.170	71	n.d.	180.6	n.d.	150094	n.d.	n.d.	296	0.057	45	n.d.	71952
Ep-05	485883	9007322	300	1767	207	n.d.	106467	0.91	n.d.	6.1	10.7	n.d.	1172	0.027	84	n.d.	12.3	n.d.	137144	n.d.	n.d.	148	0.013	59	n.d.	85537
Ep-06	486130	9007086	300	2054	223	n.d.	105838	1.37	n.d.	3.9	4.3	n.d.	1383	0.054	121	n.d.	14.4	n.d.	123487	n.d.	n.d.	462	0.019	44	n.d.	100108
Ep-07	485919	9006964	610	2117	192	n.d.	100100	n.d.	n.d.	5.9	1.6	n.d.	1521	0.210	174	n.d.	8.3	n.d.	154097	n.d.	n.d.	198	0.100	38	n.d.	152595
Ep-08	485751	9006859	300	2192	172	n.d.	85180	1.05	n.d.	n.d.	1.5	n.d.	2048	0.024	134	n.d.	6.3	n.d.	184259	n.d.	n.d.	39	n.d.	55	n.d.	145528
Ep-09	485011	9011502	300	2581	213	n.d.	104760	n.d.	n.d.	n.d.	4.9	0.054	1516	n.d.	112	n.d.	9.0	n.d.	167495	n.d.	n.d.	47	n.d.	36	n.d.	143003
Ep-10	485007	9011760	300	2832	168	n.d.	109780	n.d.	n.d.	10.7	4.0	n.d.	3548	n.d.	118	n.d.	13.7	n.d.	155593	n.d.	n.d.	137	n.d.	26	n.d.	141469
Ep-11	484951	9012003	300	3079	192	0.083	100020	n.d.	n.d.	7.0	3.6	n.d.	2352	0.062	151	n.d.	222.1	n.d.	162683	n.d.	n.d.	109	0.019	53	n.d.	157476
Ep-12	485333	9009875	300	976	338	n.d.	116100	n.d.	n.d.	4.9	4.9	n.d.	n.d.	0.049	6	n.d.	14.3	n.d.	154219	n.d.	n.d.	270	0.050	10	n.d.	162088
Ep-18	485875	9008347	300	853	296	n.d.	101575	0.67	n.d.	3.0	1.0	n.d.	240	0.028	11	n.d.	1.7	n.d.	104746	n.d.	n.d.	72	n.d.	3	n.d.	177528
SBD018-496.6	485615	9009036	33	121	235	n.d.	108303	0.46	n.d.	2.8	2.3	n.d.	494	0.026	100	1.8	68.7	n.d.	129013	86	n.d.	81	0.007	29	n.d.	142472
SBD018-619	485615	9009112	-64	160	235	n.d.	95380	0.59	n.d.	2.8	10.4	n.d.	811	0.045	98	1.8	7.4	n.d.	107702	57	n.d.	1111	0.038	36	n.d.	156547
SBD021-522.8	485633	9009146	21	197	261	n.d.	106944	1.30	n.d.	4.0	3.6	n.d.	510	0.095	100	1.3	15.8	n.d.	139619	74	n.d.	894	0.072	35	n.d.	127659
SBD130-21	484960	9008600	513	1134	270	n.d.	106329	0.37	n.d.	0.7	0.055	447	0.022	n.d.	n.d.	13.3	13.3	n.d.	123059	42	n.d.	19	n.d.	n.d.	0.002	176567
SBD143-41	484715	9008462	531	952	209	n.d.	115095	0.54	0.019	n.d.	7.9	n.d.	1700	0.129	n.d.	n.d.	4.6	0.021	160254	37	0.039	46	0.033	n.d.	0.010	136659
SBD143-49	484715	9008462	523	952	273	n.d.	120244	0.84	0.011	n.d.	4.6	n.d.	949	0.140	n.d.	n.d.	4.9	0.056	168068	34	0.038	31	0.071	n.d.	0.028	122395

SBD145-33	484841	9008488	521	835	281	n.d.	107951	0.42	n.d.	n.d.	0.7	n.d.	345	0.032	n.d.	n.d.	3.1	0.024	161155	36	n.d.	27	0.014	n.d.	0.004	154238
SBD145-73.2	484841	9008488	481	835	281	n.d.	107823	0.52	n.d.	n.d.	0.8	0.008	519	0.011	n.d.	n.d.	1.9	n.d.	164200	37	0.020	42	n.d.	n.d.	0.005	155523
SBD145-83	484841	9008488	471	835	315	n.d.	117237	0.50	n.d.	n.d.	0.7	0.036	547	0.009	n.d.	n.d.	3.0	0.008	163350	37	0.011	32	0.008	n.d.	n.d.	151333
SBD256-813	485607	9009204	-348	230	260	n.a.	n.a.	n.a.	n.a.	n.a.	n.a.	n.a.	n.a.	n.a.	n.a.	n.a.	n.a.	n.a.	n.a.	n.a.	n.a.	n.a.	n.a.	n.a.	n.a.	n.a.
SBD257-0965.6	485633	9008893	-520	170	265	0.034	104331	0.40	n.d.	2.0	4.0	n.d.	629	0.153	64	1.8	1.3	n.d.	118972	58	n.d.	47	0.043	15	n.d.	142089
SBD276-876.4	485628	9009275	-432	304	n.c.	n.a.	n.a.	n.a.	n.a.	n.a.	n.a.	n.a.	n.a.	n.a.	n.a.	n.a.	n.a.	n.a.	n.a.	n.a.	n.a.	n.a.	n.a.	n.a.	n.a.	n.a.
SBD276-912.6	485629	9009258	-464	289	n.c.	n.a.	n.a.	n.a.	n.a.	n.a.	n.a.	n.a.	n.a.	n.a.	n.a.	n.a.	n.a.	n.a.	n.a.	n.a.	n.a.	n.a.	n.a.	n.a.	n.a.	n.a.
SBD284-100	484945	9008575	423	699	n.c.	n.d.	100000	0.24	n.d.	n.d.	0.2	n.d.	293	0.053	n.d.	n.d.	0.5	0.012	132811	48	n.d.	54	0.016	n.d.	0.005	17139
SBD284-1124	485404	9008916	-423		n.c.	n.a.	n.a.	n.a.	n.a.	n.a.	n.a.	n.a.	n.a.	n.a.	n.a.	n.a.	n.a.	n.a.	n.a.	n.a.	n.a.	n.a.	n.a.	n.a.	n.a.	n.a.
SBD284-1145	485415	9008924	-439	120	252	n.a.	n.a.	n.a.	n.a.	n.a.	n.a.	n.a.	n.a.	n.a.	n.a.	n.a.	n.a.	n.a.	n.a.	n.a.	n.a.	n.a.	n.a.	n.a.	n.a.	n.a.
SBD284-17.5	484911	9008549	493	742	290	n.d.	107683	0.43	n.d.	n.d.	1.7	0.021	404	0.009	n.d.	n.d.	3.4	0.007	166183	34	0.014	16	0.006	n.d.	0.002	153368
SBD284-170	484973	9008596	363	1011	276	n.d.	105848	0.22	n.d.	n.d.	0.2	n.d.	392	0.035	n.d.	n.d.	1.8	0.007	121615	50	n.d.	34	0.011	n.d.	0.003	184426
SBD284-175.8	484975	9008598	358	661	284	n.d.	107014	0.26	n.d.	n.d.	0.2	n.d.	483	0.022	n.d.	n.d.	0.8	0.013	117197	72	0.057	23	n.d.	n.d.	0.013	187447
SBD284-20	484912	9008549	492	741	299	n.d.	110508	0.40	n.d.	n.d.	0.5	0.003	248	0.009	n.d.	n.d.	0.4	n.d.	154998	38	n.d.	18	0.009	n.d.	n.d.	152484
SBD284-226	484995	9008614	315	636	183	n.d.	109790	n.d.	n.d.	n.d.	0.4	n.d.	432	0.022	n.d.	n.d.	2.3	0.011	107459	50	n.d.	50	n.d.	n.d.	0.004	191738
SBD284-233	484998	9008616	309	950	283	n.d.	106768	0.45	n.d.	n.d.	0.2	n.d.	255	0.050	n.d.	n.d.	3.2	n.d.	194032	21	n.d.	15	0.019	n.d.	n.d.	130420
SBD284-266	485011	9008626	280	917	268	n.d.	102068	0.27	n.d.	n.d.	0.1	n.d.	252	0.006	n.d.	n.d.	0.8	0.004	131315	39	n.d.	10	n.d.	n.d.	n.d.	177645
SBD284-306	485027	9008638	246	596	266	n.d.	105267	n.d.	n.d.	n.d.	0.6	n.d.	2445	0.112	n.d.	n.d.	6.0	0.065	129386	73	0.078	62	0.029	n.d.	0.057	194653
SBD284-375	485054	9008659	185	811	347	n.d.	117801	n.d.	n.d.	n.d.	3.4	n.d.	3200	0.138	n.d.	n.d.	8.0	0.025	126304	35	n.d.	518	0.051	n.d.	n.d.	181771
SBD284-423	485073	9008675	150	769	n.c.	n.a.	n.a.	n.a.	n.a.	n.a.	n.a.	n.a.	n.a.	n.a.	n.a.	n.a.	n.a.	n.a.	n.a.	n.a.	n.a.	n.a.	n.a.	n.a.	n.a.	n.a.
SBD284-424	485073	9008675	143	764	153	n.d.	111031	n.d.	n.d.	n.d.	0.8	n.d.	200	0.019	n.d.	n.d.	0.4	n.d.	131961	62	n.d.	20	n.d.	n.d.	n.d.	185775
SBD284-535	485118	9008713	57	662	n.c.	n.a.	n.a.	n.a.	n.a.	n.a.	n.a.	n.a.	n.a.	n.a.	n.a.	n.a.	n.a.	n.a.	n.a.	n.a.	n.a.	n.a.	n.a.	n.a.	n.a.	n.a.
SBD284-775	485227	9008792	-149	343	n.c.	n.a.	n.a.	n.a.	n.a.	n.a.	n.a.	n.a.	n.a.	n.a.	n.a.	n.a.	n.a.	n.a.	n.a.	n.a.	n.a.	n.a.	n.a.	n.a.	n.a.	n.a.
SBD284-840	485260	9008815	-200	363	n.c.	n.a.	n.a.	n.a.	n.a.	n.a.	n.a.	n.a.	n.a.	n.a.	n.a.	n.a.	n.a.	n.a.	n.a.	n.a.	n.a.	n.a.	n.a.	n.a.	n.a.	n.a.
SBD284-95	484943	9008573	428	702	318	n.d.	108852	0.25	n.d.	n.d.	0.4	n.d.	331	0.022	n.d.	n.d.	0.6	0.018	125913	44	n.d.	39	0.010	n.d.	0.005	176224
SBD284-965.5	485323	9008860	-300	247	270	n.a.	n.a.	n.a.	n.a.	n.a.	n.a.	n.a.	n.a.	n.a.	n.a.	n.a.	n.a.	n.a.	n.a.	n.a.	n.a.	n.a.	n.a.	n.a.	n.a.	n.a.
SBD284-965.6	485323	9008860	-300	208	n.c.	n.a.	n.a.	n.a.	n.a.	n.a.	n.a.	n.a.	n.a.	n.a.	n.a.	n.a.	n.a.	n.a.	n.a.	n.a.	n.a.	n.a.	n.a.	n.a.	n.a.	n.a.
SBD284-97	484943	9008574	426	1083	295	n.d.	108806	0.23	n.d.	n.d.	0.4	0.004	454	0.017	n.d.	n.d.	0.6	0.006	121590	37	n.d.	29	0.008	n.d.	0.005	180049
SBD299-0772.5	485540	9009360	-221	363	n.c.	n.a.	n.a.	n.a.	n.a.	n.a.	n.a.	n.a.	n.a.	n.a.	n.a.	n.a.	n.a.	n.a.	n.a.	n.a.	n.a.	n.a.	n.a.	n.a.	n.a.	n.a.
SBD304-619.6	485621	9008676	-258	346	271	n.a.	n.a.	n.a.	n.a.	n.a.	n.a.	n.a.	n.a.	n.a.	n.a.	n.a.	n.a.	n.a.	n.a.	n.a.	n.a.	n.a.	n.a.	n.a.	n.a.	n.a.
B2-0.3*	483270	9007990	520	2448	n.c.	n.d.	108756	0.87	0.024	n.d.	10.4	0.006	1360	0.055	n.d.	n.d.	3.2	0.015	167083	31	0.022	53	0.018	n.d.	0.019	145884
B2-11.9*	482933	9008262	380	2671	n.c.	n.d.	100000	0.55	0.019	n.d.	7.5	0.133	1235	0.015	n.d.	n.d.	629.7	0.009	154582	27	0.015	111	0.022	n.d.	0.007	105138
B2-23.0*	483279	9007982	520	2611	n.c.	n.d.	100000	0.39	n.d.	n.d.	6.1	0.010	1707	0.013	n.d.	n.d.	1229.4	n.d.	159198	25	n.d.	46	0.010	n.d.	n.d.	102479
B3-3.2*	483287	9007975	520	2607	n.c.	n.d.	100000	0.79	n.d.	n.d.	11.6	n.d.	1166	0.034	n.d.	n.d.	2.4	0.023	150864	30	0.087	244	0.012	n.d.	0.010	99504
BH04-45*	483175	9008140	467	2626	n.c.	n.d.	89048	n.d.	n.d.	n.d.	0.3	n.d.	3265	n.d.	n.d.	n.d.	22.4	n.d.	140213	41	n.d.	79	n.d.	n.d.	0.006	149118
BH04-48A*	483305	9007950	-	2466	n.c.	n.a.	n.a.	n.a.	n.a.	n.a.	n.a.	n.a.	n.a.	n.a.	n.a.	n.a.	n.a.	n.a.	n.a.	n.a.	n.a.	n.a.	n.a.	n.a.	n.a.	n.a.
BH05-70B†	479560	9008695	213	2352	209	n.d.	96882	0.79	n.d.	3.5	4.0	0.994	1978	0.200	59	6.9	24.9	n.d.	130949	56	n.d.	92	0.060	26	n.d.	140806
BH05-71†	480050	9008240	119	2909	235	n.d.	100619	0.61	n.d.	2.6	0.5	0.007	481	0.066	118	1.7	1.6	n.d.	120254	52	n.d.	112	0.078	15	n.d.	151602
BH05-72†	479325	9009100	300	1928	249	0.018	104008	0.70	n.d.	5.3	0.5	n.d.	811	0.023	47	9.1	4.1	n.d.	160016	43	n.d.	235	n.d.	28	n.d.	128647
BH05-73†	479300	9009665	460	1367	212	n.d.	98987	2.25	n.d.	5.0	0.4	0.011	22499	0.823	89	30.3	247.9	n.d.	187566	59	n.d.	467	0.187	17	n.d.	135002
BH05-74†	479425	9008955	265	2079	197	0.036	93031	1.25	n.d.	1.6	3.0	0.032	630	0.321	163	6.2	278.7	n.d.	125039	45	n.d.	118	0.099	20	n.d.	147905
BH05-75†	479335	9009830	552	1218	273	n.d.	108193	0.32	n.d.	n.d.	1.2	0.010	258	0.045	n.d.	n.d.	0.8	0.010	130114	46	0.007	112	0.014	n.d.	0.003	177868
BH05-76†	479230	9009290	342	1736	186	n.d.	96737	n.d.	n.d.	3.8	13.0	n.d.	2385	0.145	103	12.7	526.6	n.d.	134484	33	n.d.	721	0.060	13	n.d.	130467
BH05-77†	479395	9010215	463	825	145	n.d.	84919	0.49	n.d.	3.7	87.6	n.d.	2860	0.104	156	2.2	53.9	n.d.	152865	39	n.d.	1440	0.061	21	n.d.	121651
BH05-78†	479410	9010410	423	638	215	0.043	110167	3.06	n.d.	3.8	7.8	0.040	895	0.784	59	4.0	59.4	n.d.	118620	47	n.d.	76	0.174	8	n.d.	129400
BH05-79†	479390	9010115	487	934	222	n.d.	95844	0.71	n.d.	3.8	1.3	n.d.	1030	0.173	94	4.8	10.9	n.d.	138762	36	n.d.	34	0.058	10	n.d.	124826
BH05-80†	479680	9008460	174	2603	254	n.d.	101955	0.61	n.d.	3.8	3.0	0.030	1445	0.044	86	8.0	5.5	n.d.	121156	42	n.d.	44	0.015	14	n.d.	137416

§Chlorite crystallization temperature calculated using the thermodynamic model of Walshe (1986) using major element oxide data derived from microprobe.

(continued on next page)

*Sample proximal to Bambu epithermal system.

†Sample proximal to Sekongkang porphyry prospect.

‡Distance calculated from Sekongkang center.

n.a. - not analysed.

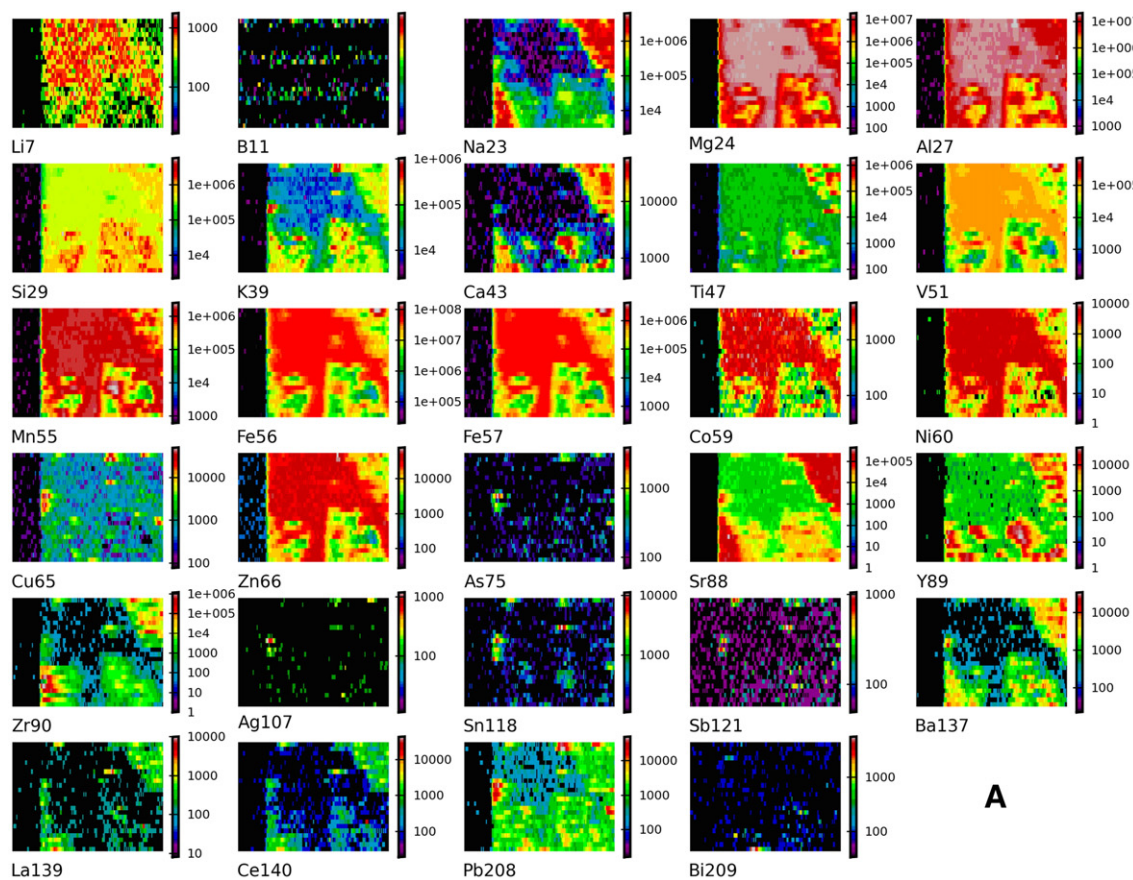
n.d. - not determined.

n.c. - not computed (due to insufficient analyses and/or non-convergent calculations).

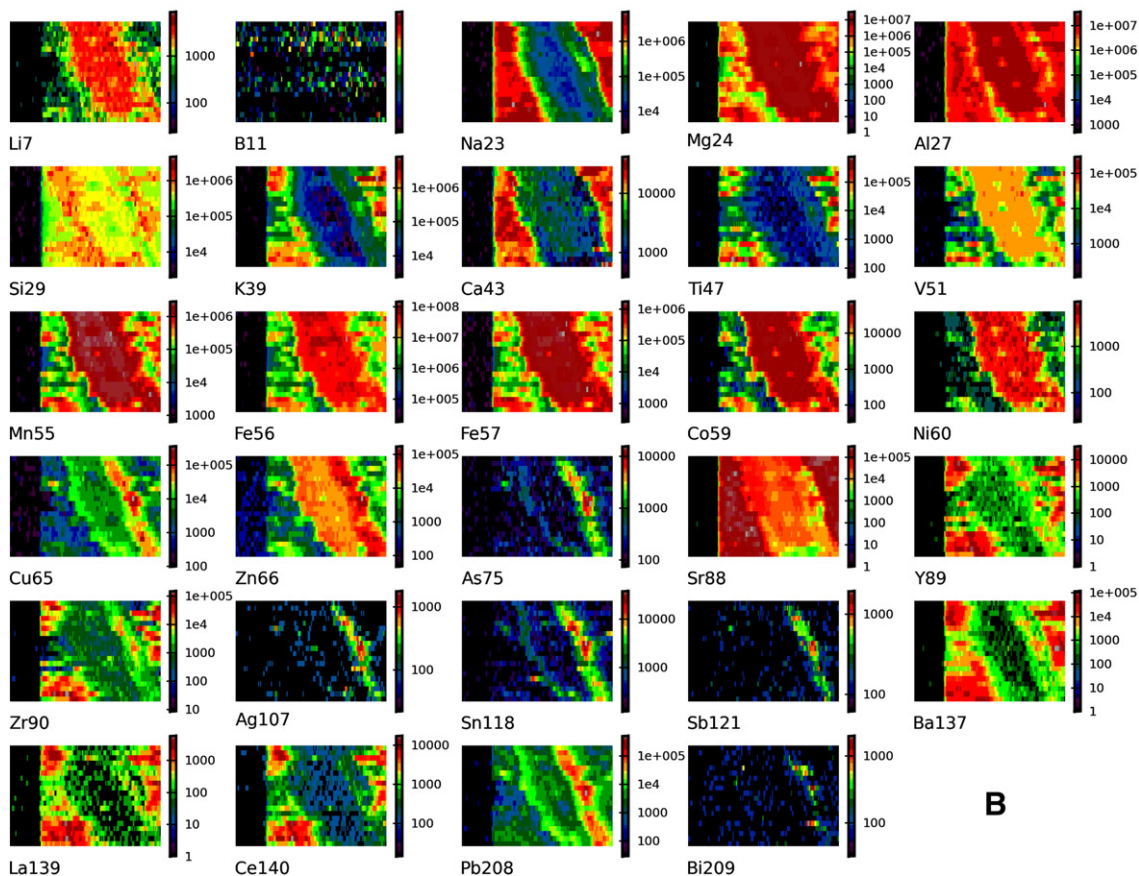
Table 1 (continued)

Sample	Mn	Mo	Na	Ni	Pb	Sb	Si	Sn	Sr	Ta	Th	Ti	Tl	U	V	Y	Yb	Zn	Zr
BH04_52	4392	n.d.	90	n.d.	0.51	0.038	n.d.	0.11	17.1	n.d.	0.013	n.d.	0.007	n.d.	95	0.32	0.072	373	1.36
BH04_53	5210	0.123	53	n.d.	1.81	n.d.	n.d.	0.19	16.9	n.d.	0.012	n.d.	0.010	0.006	135	0.31	0.058	439	0.16
BH04_54	4724	n.d.	189	n.d.	1.03	0.140	n.d.	0.18	33.9	n.d.	0.004	n.d.	0.008	0.006	115	0.11	0.013	392	0.39
BH04_55B	3707	0.082	436	n.d.	2.28	0.076	n.d.	0.42	46.8	n.d.	n.d.	n.d.	0.009	0.006	88	0.12	0.024	372	0.37
BH10-101	4128	n.d.	78	66	0.10	0.101	144517	0.71	20.1	n.d.	n.d.	20	n.d.	n.d.	196	41.32	n.d.	552	0.28
BH10-102	3893	n.d.	109	56	0.24	0.084	144642	0.69	14.8	n.d.	n.d.	25	n.d.	0.014	110	0.44	n.d.	428	0.32
BH10-103	3344	n.d.	65	122	0.39	0.329	149252	0.65	29.4	n.d.	n.d.	20	n.d.	0.012	96	1.21	n.d.	215	1.14
BH10-104	6239	n.d.	164	39	1.00	n.d.	177638	0.64	41.5	n.d.	n.d.	17	n.d.	0.013	86	111.43	n.d.	820	0.38
BH10-105	3957	n.d.	514	52	0.41	0.389	173366	0.49	84.3	n.d.	n.d.	31	n.d.	0.009	66	30.80	n.d.	498	0.83
BH10-106	3725	n.d.	242	91	1.22	0.359	168908	0.38	60.9	n.d.	n.d.	132	n.d.	0.022	57	0.55	n.d.	353	1.97
BH10-107	3708	n.d.	63	62	0.39	n.d.	169728	0.43	24.6	n.d.	n.d.	41	n.d.	n.d.	183	0.10	n.d.	361	0.38
BH10-108	5128	n.d.	62	57	0.47	0.269	183578	0.42	33.1	n.d.	n.d.	38	n.d.	n.d.	46	0.16	n.d.	827	0.79
BH10-109	3846	n.d.	208	70	0.42	n.d.	173016	0.72	72.4	n.d.	n.d.	91	n.d.	0.008	78	16.63	n.d.	207	0.99
BH10-110	3512	n.d.	44	93	0.44	0.160	157056	0.52	54.2	n.d.	n.d.	91	n.d.	n.d.	50	1.44	n.d.	174	0.42
BH10-111	2017	n.d.	204	167	0.82	0.321	161936	0.85	68.2	n.d.	n.d.	55	n.d.	0.006	53	32.62	n.d.	396	1.85
BH10-112	3070	n.d.	133	427	0.89	0.100	175619	0.76	62.0	n.d.	n.d.	112	n.d.	0.029	73	6.39	n.d.	742	1.77
BH10-113	2150	n.d.	237	70	0.29	0.167	170474	0.77	61.5	n.d.	n.d.	50	n.d.	0.008	81	0.10	n.d.	239	1.50
BH10-114	2339	n.d.	434	336	1.62	0.121	161769	3.86	51.1	n.d.	n.d.	154	n.d.	0.026	48	10.23	n.d.	322	1.85
BH10-115	947	n.d.	335	275	1.91	0.571	170417	1.23	37.7	n.d.	n.d.	1390	n.d.	0.481	150	5.90	n.d.	285	32.29
BH-17	n.a.	n.a.	n.a.	n.a.	n.a.	n.a.	n.a.	n.a.	n.a.	n.a.	n.a.	n.a.	n.a.	n.a.	n.a.	n.a.	n.a.	n.a.	n.a.
BH-18	n.a.	n.a.	n.a.	n.a.	n.a.	n.a.	n.a.	n.a.	n.a.	n.a.	n.a.	n.a.	n.a.	n.a.	n.a.	n.a.	n.a.	n.a.	n.a.
BH-19	4109	n.d.	36	n.d.	0.21	0.096	n.d.	0.38	5.9	n.d.	0.017	n.d.	0.012	0.008	455	0.73	0.102	360	0.14
BH-20	n.a.	n.a.	n.a.	n.a.	n.a.	n.a.	n.a.	n.a.	n.a.	n.a.	n.a.	n.a.	n.a.	n.a.	n.a.	n.a.	n.a.	n.a.	n.a.
BH-21	4523	0.121	32	n.d.	0.44	0.089	n.d.	0.13	4.5	0.006	0.008	n.d.	0.004	0.005	284	0.09	0.015	433	0.12
BH-22	4865	n.d.	35	n.d.	0.04	n.d.	n.d.	0.23	2.2	n.d.	n.d.	n.d.	n.d.	n.d.	285	0.03	0.038	579	0.05
BH-23	n.a.	n.a.	n.a.	n.a.	n.a.	n.a.	n.a.	n.a.	n.a.	n.a.	n.a.	n.a.	n.a.	n.a.	n.a.	n.a.	n.a.	n.a.	n.a.
BH-24	11644	0.078	20	n.d.	0.40	n.d.	n.d.	0.34	2.1	0.025	n.d.	n.d.	0.012	0.004	271	0.96	0.095	1211	0.52
BH-25	4025	n.d.	18	n.d.	0.67	n.d.	n.d.	0.14	3.6	0.007	n.d.	n.d.	0.011	0.004	336	0.36	0.058	377	0.07
BH-26	n.a.	n.a.	n.a.	n.a.	n.a.	n.a.	n.a.	n.a.	n.a.	n.a.	n.a.	n.a.	n.a.	n.a.	n.a.	n.a.	n.a.	n.a.	n.a.
BH-27	n.a.	n.a.	n.a.	n.a.	n.a.	n.a.	n.a.	n.a.	n.a.	n.a.	n.a.	n.a.	n.a.	n.a.	n.a.	n.a.	n.a.	n.a.	n.a.
BH-35	n.a.	n.a.	n.a.	n.a.	n.a.	n.a.	n.a.	n.a.	n.a.	n.a.	n.a.	n.a.	n.a.	n.a.	n.a.	n.a.	n.a.	n.a.	n.a.
Ep-01	4845	n.d.	18	30	0.16	0.050	116765	5.99	2.1	n.d.	n.d.	15	n.d.	n.d.	113	0.02	n.d.	651	0.07
Ep-02	4703	n.d.	22	18	0.33	0.014	117694	0.12	5.3	n.d.	n.d.	25	n.d.	n.d.	172	0.02	n.d.	623	0.10
Ep-03	4182	n.d.	28	17	0.43	0.131	135314	0.52	11.9	n.d.	n.d.	18	n.d.	n.d.	168	0.27	n.d.	434	0.10
Ep-04	4631	n.d.	74	8	0.46	0.186	138200	0.45	15.2	n.d.	n.d.	14	n.d.	n.d.	95	0.44	n.d.	515	0.17
Ep-05	2400	n.d.	31	107	0.90	0.232	136722	0.61	14.0	n.d.	n.d.	29	n.d.	n.d.	284	0.19	n.d.	484	0.19
Ep-06	4735	n.d.	38	72	0.42	n.d.	146272	0.56	14.4	n.d.	n.d.	20	n.d.	n.d.	183	0.05	n.d.	621	0.10
Ep-07	5878	n.d.	43	94	0.17	n.d.	162118	0.74	8.9	n.d.	n.d.	8	n.d.	n.d.	132	0.15	n.d.	448	0.27
Ep-08	3786	n.d.	42	61	0.24	n.d.	164240	0.68	7.1	n.d.	n.d.	9	n.d.	n.d.	130	0.36	n.d.	296	0.10
Ep-09	3432	n.d.	20	179	0.15	n.d.	159953	1.07	14.5	n.d.	n.d.	33	n.d.	n.d.	361	0.15	n.d.	335	0.23
Ep-10	4716	n.d.	59	67	0.27	0.308	170196	n.d.	11.9	n.d.	n.d.	15	n.d.	n.d.	170	0.07	n.d.	379	0.28
Ep-11	6504	n.d.	67	95	0.46	0.325	165638	1.32	9.6	n.d.	n.d.	51	n.d.	n.d.	108	0.22	n.d.	524	0.28
Ep-12	1121	n.d.	35	23	0.17	0.129	141145	0.82	0.5	n.d.	n.d.	470	n.d.	n.d.	137	0.10	n.d.	280	n.d.
Ep-18	850	n.d.	14	18	0.11	n.d.	131123	3.15	0.3	n.d.	n.d.	488	n.d.	n.d.	280	0.11	n.d.	128	n.d.
SBD018-496.6	4171	n.d.	58	26	1.35	n.d.	133592	1.82	1.4	n.d.	n.d.	345	n.d.	0.015	101	0.06	n.d.	1503	0.04
SBD018-619	4518	n.d.	256	33	1.47	n.d.	132362	1.37	5.3	n.d.	n.d.	455	n.d.	0.012	92	0.09	n.d.	827	0.12
SBD021-522.8	6408	n.d.	41	24	0.27	0.131	194744	2.76	2.1	n.d.	n.d.	477	n.d.	0.041	151	0.20	n.d.	2232	0.78
SBD130-21	4912	0.116	27	n.d.	0.66	n.d.	n.d.	0.19	8.4	n.d.	0.034	n.d.	n.d.	0.004	229	0.02	n.d.	711	0.06
SBD143-41	5479	0.103	53	n.d.	1.25	0.060	n.d.	0.52	11.4	n.d.	0.008	n.d.	0.008	0.006	304	0.44	0.057	1070	0.39
SBD143-49	8374	0.140	32	n.d.	0.70	0.075	n.d.	0.35	11.9	0.004	0.011	n.d.	0.015	0.006	254	1.68	0.200	1933	0.43

SBD145-33	5509	0.092	16	n.d.	0.94	0.028	n.d.	0.19	9.8	n.d.	n.d.	n.d.	n.d.	n.d.	256	0.39	0.034	1077	0.06
SBD145-73.2	4870	0.056	26	n.d.	0.18	0.067	n.d.	0.25	1.6	n.d.	n.d.	n.d.	n.d.	n.d.	209	0.04	n.d.	739	0.09
SBD145-83	5496	0.087	18	n.d.	0.29	n.d.	n.d.	0.15	2.7	0.006	n.d.	n.d.	0.013	n.d.	306	0.05	n.d.	779	0.05
SBD256-813	n.a.	n.a.	n.a.	n.a.	n.a.	n.a.	n.a.	n.a.	n.a.	n.a.	n.a.	n.a.	n.a.	n.a.	n.a.	n.a.	n.a.	n.a.	n.a.
SBD257-0965.6	6271	n.d.	39	18	0.16	n.d.	126795	1.10	4.0	n.d.	n.d.	244	n.d.	0.007	76	0.06	n.d.	1083	0.06
SBD276-876.4	n.a.	n.a.	n.a.	n.a.	n.a.	n.a.	n.a.	n.a.	n.a.	n.a.	n.a.	n.a.	n.a.	n.a.	n.a.	n.a.	n.a.	n.a.	n.a.
SBD276-912.6	n.a.	n.a.	n.a.	n.a.	n.a.	n.a.	n.a.	n.a.	n.a.	n.a.	n.a.	n.a.	n.a.	n.a.	n.a.	n.a.	n.a.	n.a.	n.a.
SBD284-100	2674	0.064	14	n.d.	0.14	n.d.	n.d.	0.19	0.7	0.005	n.d.	n.d.	0.011	0.005	332	0.16	0.038	480	0.02
SBD284-1124	n.a.	n.a.	n.a.	n.a.	n.a.	n.a.	n.a.	n.a.	n.a.	n.a.	n.a.	n.a.	n.a.	n.a.	n.a.	n.a.	n.a.	n.a.	n.a.
SBD284-1145	n.a.	n.a.	n.a.	n.a.	n.a.	n.a.	n.a.	n.a.	n.a.	n.a.	n.a.	n.a.	n.a.	n.a.	n.a.	n.a.	n.a.	n.a.	n.a.
SBD284-17.5	5565	0.106	11	n.d.	1.07	n.d.	n.d.	0.10	3.9	n.d.	n.d.	n.d.	0.005	n.d.	269	0.05	0.016	994	0.05
SBD284-170	2098	0.087	21	n.d.	1.38	n.d.	n.d.	0.20	0.7	n.d.	n.d.	n.d.	0.011	n.d.	371	0.07	n.d.	303	0.03
SBD284-175.8	1760	0.060	24	n.d.	0.03	0.031	n.d.	0.16	0.7	n.d.	n.d.	n.d.	n.d.	n.d.	282	0.20	0.047	220	0.09
SBD284-20	5299	0.095	9	n.d.	0.14	0.024	n.d.	0.17	2.0	n.d.	n.d.	n.d.	n.d.	n.d.	241	0.03	0.021	789	0.05
SBD284-226	2239	n.d.	55	n.d.	0.04	n.d.	n.d.	0.45	0.7	n.d.	0.005	n.d.	0.021	n.d.	296	0.10	0.026	222	0.04
SBD284-233	8863	0.131	n.d.	n.d.	0.12	n.d.	n.d.	0.11	0.5	n.d.	0.003	n.d.	n.d.	n.d.	152	n.d.	n.d.	704	n.d.
SBD284-266	1625	0.064	12	n.d.	0.02	n.d.	n.d.	n.d.	0.6	n.d.	n.d.	n.d.	0.006	n.d.	200	0.03	n.d.	282	n.d.
SBD284-306	2088	n.d.	100	n.d.	0.14	n.d.	n.d.	0.49	0.5	n.d.	0.011	n.d.	n.d.	0.003	353	3.78	0.417	280	0.73
SBD284-375	911	n.d.	847	n.d.	0.24	n.d.	n.d.	n.d.	17.6	n.d.	n.d.	n.d.	0.060	n.d.	187	0.20	n.d.	131	n.d.
SBD284-423	n.a.	n.a.	n.a.	n.a.	n.a.	n.a.	n.a.	n.a.	n.a.	n.a.	n.a.	n.a.	n.a.	n.a.	n.a.	n.a.	n.a.	n.a.	n.a.
SBD284-424	1086	n.d.	n.d.	n.d.	n.d.	n.d.	n.d.	0.14	0.6	n.d.	n.d.	n.d.	n.d.	n.d.	221	0.09	n.d.	196	n.d.
SBD284-535	n.a.	n.a.	n.a.	n.a.	n.a.	n.a.	n.a.	n.a.	n.a.	n.a.	n.a.	n.a.	n.a.	n.a.	n.a.	n.a.	n.a.	n.a.	n.a.
SBD284-775	n.a.	n.a.	n.a.	n.a.	n.a.	n.a.	n.a.	n.a.	n.a.	n.a.	n.a.	n.a.	n.a.	n.a.	n.a.	n.a.	n.a.	n.a.	n.a.
SBD284-840	n.a.	n.a.	n.a.	n.a.	n.a.	n.a.	n.a.	n.a.	n.a.	n.a.	n.a.	n.a.	n.a.	n.a.	n.a.	n.a.	n.a.	n.a.	n.a.
SBD284-95	3663	0.097	14	n.d.	0.06	0.029	n.d.	0.19	1.0	n.d.	n.d.	n.d.	0.007	n.d.	297	0.28	0.033	518	0.03
SBD284-965.5	n.a.	n.a.	n.a.	n.a.	n.a.	n.a.	n.a.	n.a.	n.a.	n.a.	n.a.	n.a.	n.a.	n.a.	n.a.	n.a.	n.a.	n.a.	n.a.
SBD284-965.6	n.a.	n.a.	n.a.	n.a.	n.a.	n.a.	n.a.	n.a.	n.a.	n.a.	n.a.	n.a.	n.a.	n.a.	n.a.	n.a.	n.a.	n.a.	n.a.
SBD284-97	3148	0.058	22	n.d.	0.07	n.d.	n.d.	0.10	1.6	0.002	0.006	n.d.	0.008	0.004	321	0.10	0.019	504	0.03
SBD299-0772.5	n.a.	n.a.	n.a.	n.a.	n.a.	n.a.	n.a.	n.a.	n.a.	n.a.	n.a.	n.a.	n.a.	n.a.	n.a.	n.a.	n.a.	n.a.	n.a.
SBD304-619.6	n.a.	n.a.	n.a.	n.a.	n.a.	n.a.	n.a.	n.a.	n.a.	n.a.	n.a.	n.a.	n.a.	n.a.	n.a.	n.a.	n.a.	n.a.	n.a.
B2-0.3*	4918	0.384	32	n.d.	1.09	0.085	n.d.	0.36	6.7	0.004	0.023	n.d.	0.022	0.004	346	0.55	0.101	495	0.22
B2-11.9*	6843	0.149	745	n.d.	153.20	0.097	n.d.	0.21	10.0	0.008	0.009	n.d.	n.d.	0.004	284	0.16	0.034	3711	0.09
B2-23.0*	8860	0.078	881	n.d.	9.11	0.042	n.d.	0.07	9.2	n.d.	0.003	n.d.	n.d.	n.d.	234	0.24	0.019	4502	0.14
B3-3.2*	5391	0.131	18	n.d.	3.93	0.186	n.d.	0.21	9.7	n.d.	0.006	n.d.	0.008	0.005	308	0.54	0.062	862	1.14
BH04-45*	4255	n.d.	104	n.d.	0.44	n.d.	n.d.	n.d.	20.4	n.d.	n.d.	n.d.	n.d.	n.d.	98	0.20	0.046	366	0.84
BH04-48A*	n.a.	n.a.	n.a.	n.a.	n.a.	n.a.	n.a.	n.a.	n.a.	n.a.	n.a.	n.a.	n.a.	n.a.	n.a.	n.a.	n.a.	n.a.	n.a.
BH05-70B†	2393	n.d.	1732	36	5.13	n.d.	140593	0.93	11.8	n.d.	n.d.	151	n.d.	n.d.	451	2.32	n.d.	438	1.27
BH05-71†	2499	n.d.	44	19	0.13	n.d.	142210	0.99	2.4	n.d.	n.d.	159	n.d.	0.007	237	0.07	n.d.	366	0.13
BH05-72†	2467	n.d.	152	22	0.40	n.d.	128587	0.71	6.6	n.d.	n.d.	123	n.d.	n.d.	355	0.04	n.d.	237	0.05
BH05-73†	2564	n.d.	530	80	0.37	0.194	178951	1.11	4.0	n.d.	n.d.	402	n.d.	0.013	377	6.92	n.d.	192	12.15
BH05-74†	3076	n.d.	80	82	8.09	0.117	127740	0.77	3.6	n.d.	n.d.	246	n.d.	0.007	245	0.49	n.d.	496	0.21
BH05-75†	2044	0.023	7	n.d.	0.07	n.d.	n.d.	0.15	1.8	n.d.	n.d.	n.d.	n.d.	n.d.	306	0.12	0.021	152	0.02
BH05-76†	3186	n.d.	411	66	0.48	n.d.	160599	0.93	14.5	n.d.	n.d.	116	n.d.	n.d.	316	0.43	n.d.	247	0.27
BH05-77†	2150	n.d.	354	51	0.23	n.d.	143608	1.02	15.2	n.d.	n.d.	222	n.d.	n.d.	130	0.97	n.d.	294	4.41
BH05-78†	3705	n.d.	50	57	0.38	0.380	147176	0.77	1.8	n.d.	n.d.	49	n.d.	0.042	387	4.23	n.d.	408	0.13
BH05-79†	2804	n.d.	65	26	0.11	n.d.	130268	0.64	2.8	n.d.	n.d.	29	n.d.	0.009	286	0.53	n.d.	363	0.30
BH05-80†	3867	n.d.	39	85	0.21	n.d.	133924	0.59	1.7	n.d.	n.d.	120	n.d.	n.d.	208	0.35	n.d.	615	0.38



A



B

and chlorite form, typically represents the most distal, weakest imprint of hydrothermal activity. Such alteration may develop in a wide range of ore deposit systems, including porphyry Cu, Cu–Mo or Cu–Au, epithermal Au–Ag, and during retrograde alteration of skarns (Cooke et al., 2014; Dilles et al., 1992; Gustafson & Hunt, 1975; Lowell & Guilbert, 1970; Meinert, 1992; Schwartz, 1947; Seedorff et al., 2005; Sillitoe, 2000, 2010; Simmons et al., 2005). Traditionally, this domain has been one of the most difficult to explore within because the weak alteration intensity commonly renders conventional geochemical and geophysical techniques ineffective for locating mineralization.

In porphyry systems, propylitic alteration is now generally regarded as temporally equivalent to the higher temperature potassic zone (e.g., Sillitoe, 2010). Propylitic alteration has been subdivided into several sub-zones (e.g., Ballantyne, 1981; Cooke et al., 2014; Norman et al., 1991), with an inner, high temperature subzone (actinolite–epidote–chlorite), grading outward into intermediate (epidote–chlorite–calcite) and then distal subzones (chlorite–calcite–hematite). These assemblages have been mapped in detail in several porphyry systems (Garwin, 2000, 2002; Norman et al., 1991) and in contemporary geothermal environments (Rae et al., 2003).

Propylitic alteration is tacitly considered to be quite well understood, yet there is a paucity of research, particularly in the recent literature, on chemical mass transfer or isotope systematics that might constrain the relative roles of magmatic, meteoric and formation waters in its development. One study of the Ann Mason porphyry in the Yerington district, Nevada, documented oxygen and hydrogen isotope compositions of propylitically altered samples that were indistinguishable from primary igneous rocks (Dilles et al., 1992), with calculated oxygen and hydrogen fluid compositions consistent with either magmatic–meteoric fluid mixtures or cooling and equilibration of magmatic fluids with country rocks. In contrast, Norman et al. (1991) showed that at Tintic, Utah, there were systematic variations in chlorite and epidote major element compositions within the various propylitic subzones and in the oxygen and hydrogen isotope compositions of altered rocks and propylitic minerals, with an outward decrease in $\delta^{18}\text{O}$ and δD . This was attributed to the mixing between unevolved meteoric water on the fringes of the system with isotopically-exchanged meteoric water in the core of the system (or possibly a late incursion of magmatic water), apparently influenced by the prevailing view at the time that meteoric waters dominated much of the life of porphyry–hydrothermal systems (Sheppard et al., 1971). Such data today would probably be interpreted as reflecting the mixing between primary magmatic waters and unevolved meteoric waters during the initial phase of potassic–propylitic alteration. At Bingham, Utah, Bowman et al. (1987) documented a number of systematic changes with increasing distance from the deposit: (1) changes in the major element composition of biotite, epidote and chlorite; (2) decreases in fluid inclusion homogenization temperatures and salinities; and (3) decreasing calculated $\delta^{18}\text{O}_{\text{H}_2\text{O}}$ and increasing $\delta\text{D}_{\text{H}_2\text{O}}$. These patterns were interpreted in terms of either mixing between magmatic fluids and an increasing proportion outwards of formation water enriched in deuterium, or isotopic exchange of meteoric water with igneous rock at low water/rock ratios over a range of temperatures. Again, the possibility that the calculated isotope compositions of fluids could be explained purely by magmatic fluids undergoing cooling and exchange with host rocks at decreasing temperature, although modeled as viable, was not considered likely.

Studies of the trace element chemistry of propylitic minerals in porphyry systems are limited. In particular, we are not aware of any detailed studies utilizing LA-ICP-MS which delivers much lower limits of detection than other routine methods. To test the potential of trace element chemistry of propylitic minerals as a monitor of hydrothermal processes in the proximal to distal alteration zones associated with intrusion-centered hydrothermal systems, we carried out a detailed study of the Batu Hijau porphyry copper–gold system on Sumbawa Island in Nusa Tenggara Barat Province, eastern Indonesia (Fig. 1).

3. Geological setting

Batu Hijau formed at ~3.7 Ma during collision between the Indian–Australian plate and the Timorese segment of the Banda arc, is possibly linked to subduction of the Roo Rise (Garwin, 2002). The Banda arc in this region consists of: (1) a Late Oligocene to Early Miocene calc-alkaline basaltic–andesitic arc (the “Old Andesites” of van Bemmelen (1949)); (2) a Middle Miocene to Pliocene calc-alkaline arc composed of basaltic to andesitic volcanic rocks and intrusions of calc-alkaline and tholeiitic affinity (Hamilton, 1979; Hutchison, 1989; Soerja-Atmadja et al., 1994); and (3) Quaternary basaltic to dacitic, and locally rhyolitic, volcanic cover. Batu Hijau is a classic example of a giant porphyry copper–gold deposit, containing 1.64 billion tonnes of ore at average grades of 0.44% Cu and 0.35 g/t Au.

The Batu Hijau district is located within a relatively uplifted block, and is within 30 km of a major arc-transverse, left-lateral oblique-slip fault zone, the trace of which coincides with the surface projection of an inferred tear or kink in the subducting slab. This fault controls the distribution of volcanosedimentary units, the location of Neogene intrusions and the present coastline of the island. The oldest exposed rock sequence comprises volcanic sandstone with minor volcanic mudstone and local limestones biostratigraphically dated at 21–15 Ma (Adams, 1984; Berggren et al., 1995). This is overlain by volcanic lithic breccia with minor volcanic sandstone and conglomerate. A variety of intermediate, hypabyssal intrusions were emplaced into this sequence between ~15 and 4 Ma (Garwin, 2000). Porphyritic hornblende tonalite was emplaced between 5.0 and 4.7 Ma, and porphyritic dacite about 3.9 Ma. At 3.8–3.7 Ma, the tonalite porphyry stock related to the Batu Hijau mineralization was emplaced. This is a subvertical, cylindrical, composite intrusion about 200–300 m in diameter, consisting of pre-mineralization “old tonalite”, syn-mineralization “intermediate tonalite” and post-main mineralization “young tonalite”. Late in the igneous evolution, an andesitic diatreme formed in the center of the Batu Hijau district.

Batu Hijau provides an ideal setting for a study of alteration mineral chemistry because it consists of a simple, strongly mineralized tonalite intrusion emplaced into a relatively homogeneous intermediate volcanic rock sequence that developed a classically zoned hydrothermal alteration pattern (Fig. 2). Alteration consists of: (1) a core of intense biotite alteration (~400 m diameter) centered on the host tonalite porphyries; (2) an outer zone of weaker secondary biotite (extending an additional 500 m); (3) a high temperature propylitic sub-zone comprising actinolite \pm epidote (veins and replacement) \pm chlorite that forms a west-northwesterly-trending zone between Batu Hijau and the Sekongkang porphyry prospect (Fig. 2); (4) an intermediate temperature, epidote (replacement of plagioclase) \pm chlorite zone that forms a broad alteration halo around the mineralized centers; and (5) a low temperature, epidote

Fig. 3. Laser ablation ICP-MS element maps of chlorite from Batu Hijau. A. Proximal sample SBD284-95-C1b, 1085 m from the deposit center, shows homogeneous chlorite grain (defined by light pink areas in Mg and Al images) which is relatively enriched in Ti and low in Ca, Sr and Ba. Note the small circle, upper-right, which indicates the presence of a pre-existing laser ablation crater from spot analysis. B. More distal sample BH04-52-C1a, 1920 m from the center, illustrates a chlorite grain (best illustrated by the red area in the Fe images) with lower Ti and higher Ca, Sr and Ba. Note the three circles in the center of the grain indicating the presence of pre-existing laser ablation craters and the artifacts that are sometimes introduced at grain boundaries.

absent, chlorite zone (Garwin, 2002; Fig. 2). Hydrothermal pyrite extends approximately 1.5 km from the deposit center (Fig. 2). A complicating factor in the alteration history of the area, in addition to the weakly mineralized Sekongkang system, includes the presence of an epithermal vein system at Bambu, ~3 km to the west-southwest of Batu Hijau (Fig. 2).

Epidote mostly occurs in the actinolite and epidote zones, where it typically occurs as patchy replacements (>20%) of plagioclase or hornblende phenocrysts or in pyrite- or quartz-bearing veins. In the outer epidote zone, less than 20% of the feldspar and mafic phenocrysts have been replaced and veins are rare, thin and discontinuous. Chlorite is observed in almost all of the rocks sampled, including slightly abnormal composition grains overprinting biotite in the inner biotite zone (see Section 5.1.1). Calcite is sporadic and the distribution irregular. Albite was rarely identified.

4. Methods

Eighty samples, principally of porphyritic andesite and volcanic lithic breccia (basalt to basaltic-andesite composition), plus two limestones and five samples of the ore-hosting tonalites, were collected from outcrop and drill core in a series of traverses away from the deposit from within the weak biotite, actinolite, epidote and chlorite propylitic sub-zones (Fig. 2). Sixty samples were subject to whole rock geochemical analysis (AA lithochemical package, ACME Laboratories, Vancouver). Sub-samples containing minerals of interest were prepared as polished resin mounts for SEM backscattered electron imaging of mineral relationships, electron microprobe wavelength dispersive analysis (EMP-WDS) and laser ablation inductively-coupled-plasma mass spectrometry (LA-ICP-MS).

Major and minor elements in individual chlorite grains were determined using a Cameca SX100 electron microprobe housed in the Central Science Laboratories at the University of Tasmania. Major, minor and trace elements in the same grains were measured using a New Wave 193 nm solid-state laser coupled to an Agilent 7500cs quadrupole mass spectrometer, located in the School of Physical Sciences, Discipline of Earth Sciences, University of Tasmania. Typically, 5–10 spot analyses were acquired from each sample, from within 3–5 separate chlorite grains. In total, 527 LA-ICP-MS spot analyses meeting quality control criteria were obtained. Aluminium concentration determined by microprobe was used as the internal standard and NIST612 standard reference material was used for external calibration of the LA-ICP-MS results according to standard practice.

5. Results

Using standard classification criteria, chlorite compositions determined by microprobe correspond to ripidolites, with (on average) equimolar proportions of Fe and Mg ($\text{Fe/Fe} + \text{Mg} = 0.51 \pm 0.07$ (1σ)). The only minor element consistently detected by microprobe was Mn with an average concentration of 0.44 wt.%. Laser ablation ICP-MS results are summarized as sample averages in Table 1. LA-ICP-MS detected Li, Na, Mg, Al, Si, K, Ca, Ti, V, Mn, Fe, Co, Ni, Cu, Zn, Ga, Sr, Y, Ba and Pb in more than 75% of the analyses and therefore these elements were the focus of the spatial interrogation of the data.

Backscattered electron imaging and laser ablation element maps of chlorite grains show that they are internally homogeneous (Fig. 3) and that distinct variations in trace element chemistry probably reflect true substitution into the crystal lattice, rather than the presence of microinclusions. This is supported by the flat traces typically observed during LA-ICP-MS spot analysis. Inclusions of other minerals, particularly calcite, titanite and zircon, were encountered but these parts of the signal were avoided during signal integration or, if heavily contaminated, the analysis was discarded.

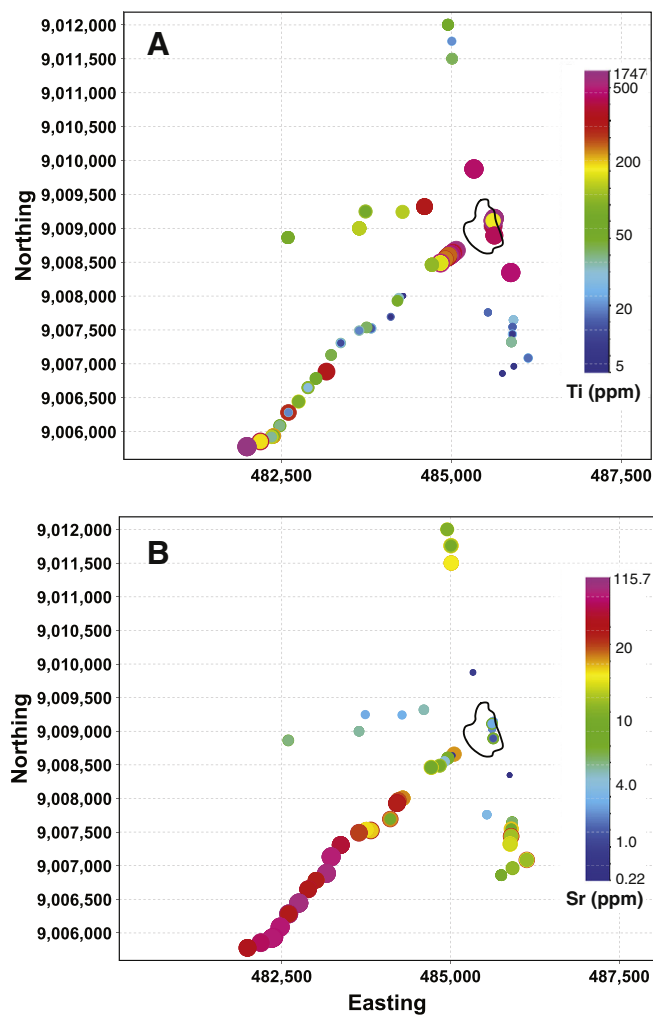


Fig. 4. Maps showing variation in mean concentrations of trace elements in chlorite in relation to Batu Hijau center (strong biotite alteration zone shown). A. Titanium shows enrichment proximal to the hydrothermal center. B. Strontium shows depletion proximal to the center. Samples that do not follow a systematic pattern exist in the distal part of the southwest traverse, beyond ~3 km from Batu Hijau (see text). Multiple analyses within individual samples are shown as stacked circles with the smallest on top. Some samples contain chlorite grains that fall within more than one bin range.

5.1. Spatial variations in chlorite composition

5.1.1. Major and trace element concentrations

In map view, a number of chlorite compositional parameters show systematic spatial variability relative to the Batu Hijau center, particularly within a 2.5 km radius of the deposit. Notably, Ti and Sr are enriched and depleted respectively in chlorite proximal to the deposit (Fig. 4). Inspection of the Ti data suggests that samples located at distances greater than 3 km from Batu Hijau along the southwest sampling traverse do not fit the systematic pattern around the deposit and may be related to other factors (e.g., a protolith control, or proximity to an unknown, buried intrusion). The data also indicate that Ti concentrations are relatively high at a given distance from the deposit on the western sampling traverse; conversely, Sr concentrations are unusually low on this traverse. This suggests a degree of asymmetry in the pattern of trace element substitution in propylitic chlorite around Batu Hijau.

Plotting element concentrations as a function of radial distance from the center of the porphyry system reveals a number of

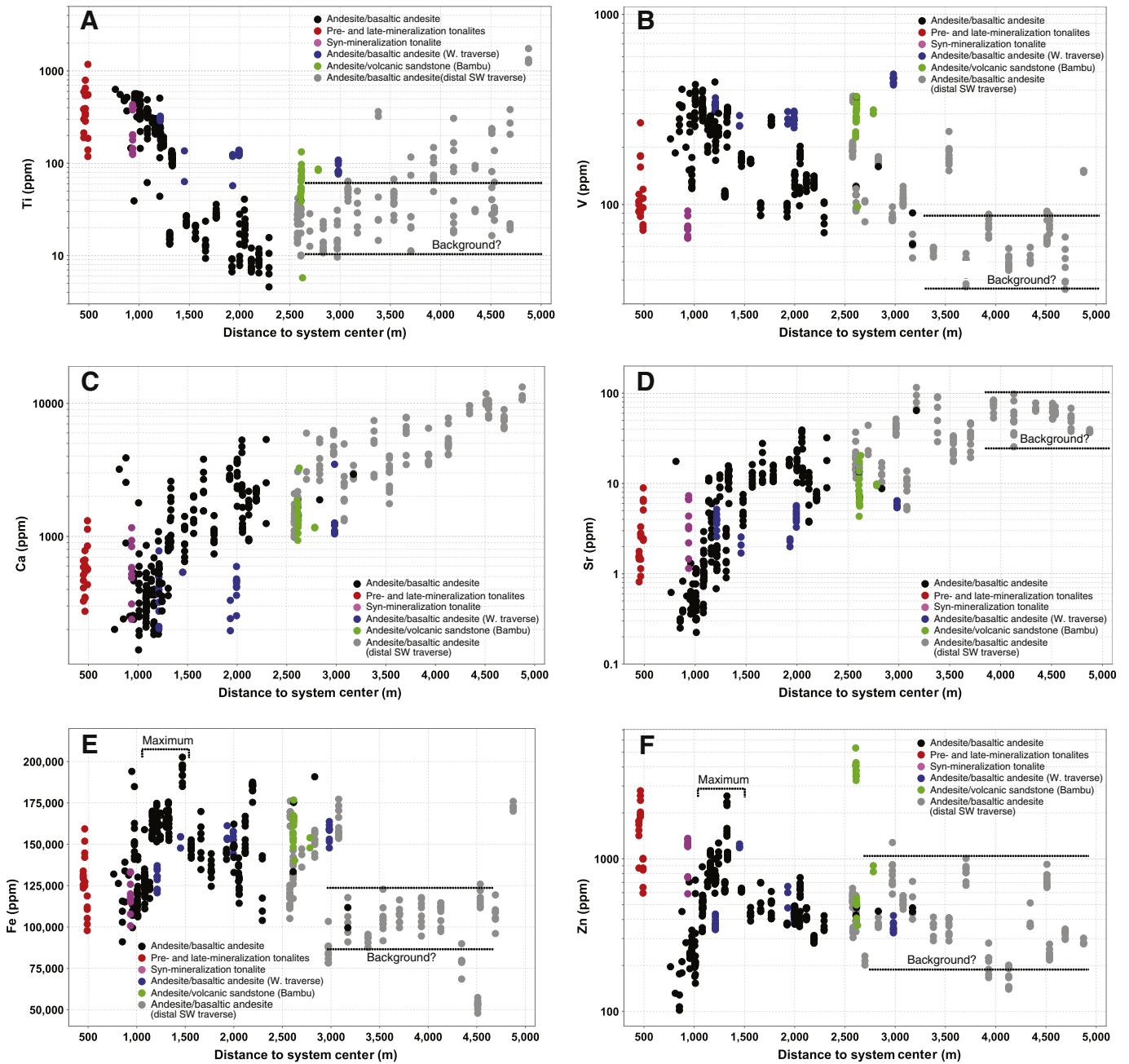


Fig. 5. Plots of element concentrations in chlorite as a function of radial distance from the Batu Hijau center. A. Group 1 element, titanium. B. Group 1 element, vanadium. C. Group 2 element, calcium. D. Group 2 element, strontium. E. Group 3 element, iron. F. Group 3 element, zinc.

patterns (Fig. 5). These can be divided into: (1) decreasing outward; (2) increasing outward; and (3) displaying a marked shoulder, or maximum, at a certain distance from the center of the system. Among group 1 elements, the most pronounced trend is the enrichment of Ti in proximal chlorite (Fig. 5A), which is mirrored by Mg. Other elements that decrease outward but with a greater degree of scatter are Al and V (Fig. 5B). In group 2, Li concentrations in chlorite increase sharply with distance in the more proximal samples and then level off, whereas Ca (Fig. 5C), Sr (Fig. 5D) and Ba appear to rapidly increase to about 1.5 km (similar to Li), with a lower rate of increase out to the limit of sampling (5 km). Boron shows a slight increase out to about 3 km. Group 3 elements are principally Mn, Fe (Fig. 5E) and Zn (Fig. 5F) which show evidence

for an enrichment halo, or annulus, with peak concentrations at a distance of 1–1.5 km. Similar patterns of proximal Mg enrichment and more distal Fe and Mn enrichment in chlorite, determined by microprobe analysis, were previously reported from the Southwest Tintic district (Norman et al., 1991).

Chlorite compositions for a number of samples plot off the trends defined by the majority of the data and these are highlighted in Fig. 5. These include the most proximal samples, hosted by the pre- and post-mainstage mineralization tonalites from within 500 m of the center of the Batu Hijau orebody (which also yielded anomalous chlorite crystallization temperatures), samples from the vicinity of the Bambu epithermal veins, and samples from the western traverse as noted for Ti and Sr above.

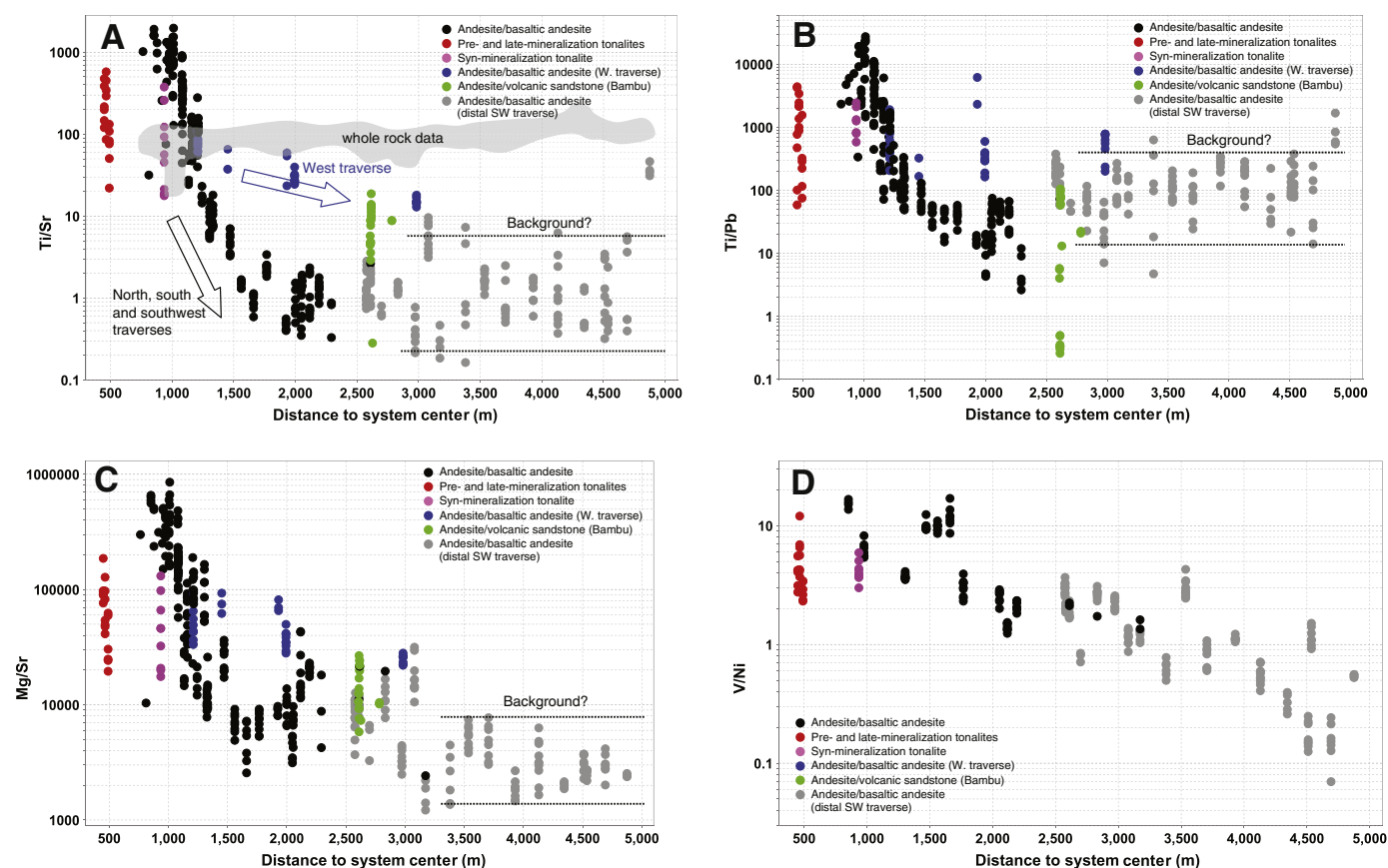


Fig. 6. Plots of element concentration ratios in chlorite as a function of radial distance from the Batu Hijau center. A. Ti/Sr ratio. Gray shaded field shows whole rock ratio data for comparison. Different trends as a function of traverse direction (see Fig. 2) are highlighted. B. Ti/Pb ratio. C. Mg/Sr ratio. D. V/Ni ratio.

5.1.2. Major and trace element ratios

In order to enhance compositional variations for the purposes of exploration applications, elements showing decreasing concentration outward patterns were ratioed to those showing increasing concentration outward patterns. These ratios typically decay exponentially as a function of distance out to a certain radius, at which point they stabilize at what is assumed to be the limit of the imprint of hydrothermal alteration where a transition to “background” occurs (Fig. 6). These ratios vary over a significant range of up to four orders of magnitude within the chlorite compositional halo attributable to the Batu Hijau center and show good exponential fit statistics with r^2 values of 0.65 to 0.82. Most ratios

show systematic decreases out to ~2.5 km but some appear to extend further, to ~5 km (Table 2).

It is noteworthy that the slope of the exponential relationship appears to be a function of the orientation of the sample transect with respect to the Batu Hijau center. Traverses to the north, south and southwest of Batu Hijau display similar steep slopes whereas the series of samples to the west, following the inner propylitic (actinolite- ± epidote- ± chlorite) alteration zone noted earlier (Fig. 2), define a shallower slope (e.g., Fig. 6A). This behavior is

Table 2
Element ratios in chlorite and exponential fit parameters as a function of distance from the Batu Hijau center.

Ratio	Orders of magnitude variation	Maximum resolvable distance (km)	Regression distance range (m)	R^2	Exponent constant (b)	Scalar constant (a)
Ti/Ni	2.5	2.5	853–2192	0.82	−0.0039	4.7×10^2
Ti/Sr	3.5	2.5	764–1767	0.77	−0.0088	3.0×10^6
Ti/Li	3	2.5	764–2192	0.72	−0.0041	7.6×10^2
Ti/Pb	3	2.5	764–1767	0.71	−0.0074	6.0×10^6
V/Ni	2	5	853–4875	0.69	−0.0009	2.0×10^1
Ti/Ba	3	4	764–1767	0.67	−0.0076	1.0×10^6
Ti/K	2.5	3	764–1767	0.67	−0.0062	6.4×10^3
Ti/Co	3	2.5	764–2192	0.67	−0.0044	5.0×10^2
Mg/Ca	2	5	764–4875	0.66	−0.0009	7.2×10^2
Mg/Sr	2	2	764–1767	0.65	−0.0051	3.0×10^7
Mg/Sr	2.5	5	764–4875	0.60	−0.0011	2.1×10^5

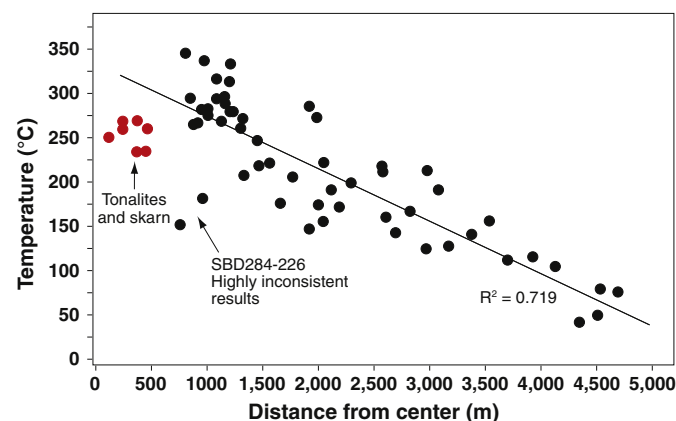


Fig. 7. Plot of chlorite geothermometer temperatures (sample average of temperatures calculated for individual microprobe spot analyses) as a function of radial distance from the Batu Hijau center. Chlorite from pre-, syn- and post-mainstage mineralization tonalites and from one skarn sample fall off the trend defined by the majority of chlorites from within the propylitic halo in the volcanic country rocks.

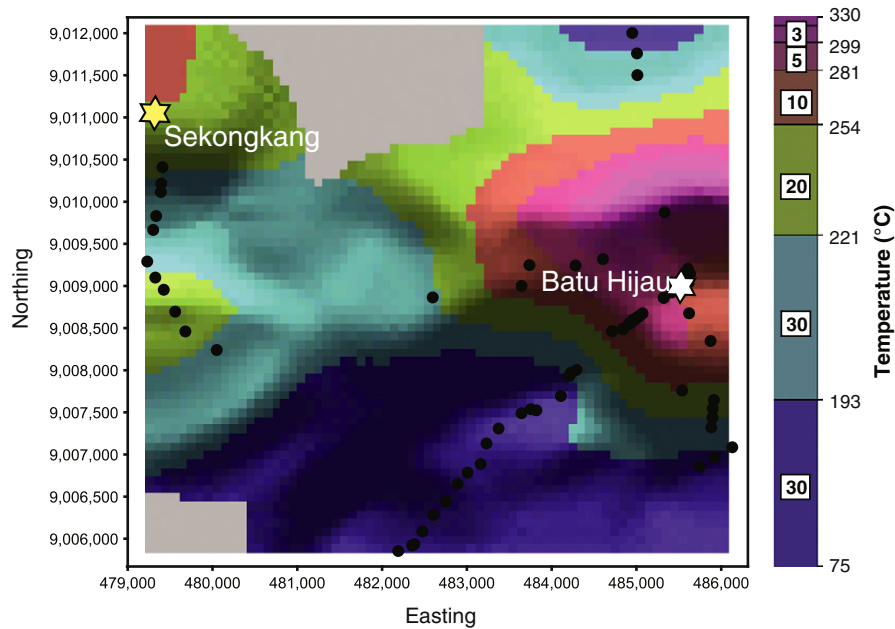


Fig. 8. Gridded map (100 m pixels) of chlorite geothermometer temperatures (sample average of temperatures calculated for individual microprobe spot analyses), shaded with a northerly light source. Light gray areas are beyond the search radius of the gridding algorithm; sample locations constraining the gridding are shown (black dots). Temperature scale is shown on the right; percentages of data in each color band are labeled. Batu Hijau center is shown by the white star; the Sekongkang prospect by the yellow star. The slight central low in the thermal maximum associated with Batu Hijau is due to the inclusion of tonalite-derived chlorite temperatures that are anomalously low. Note the lower thermal gradient (higher temperatures) along the Batu Hijau–Sekongkang trend compared with the gradients to the north and south/southwest of Batu Hijau.

consistent with a temperature control of trace element substitution, assuming that the higher temperature propylitic zone reflects the subsurface trace of a buried, elongate intrusion. If correct, these ratios effectively map out the thermal gradient around the main mineralized intrusive system at Batu Hijau, and potentially a more extensively developed underlying batholith. The changes in gradient noted in the Ca, Sr and Ba data may be reflecting both the more proximal anomaly attributable to Batu Hijau itself and the broader thermal anomaly associated with a deeper, larger scale intrusive system.

5.2. Chlorite geothermometry

To test the hypothesis that temperature is the principal control of Ti variations in chlorite, we have computed crystallization temperatures of the chlorite grains analyzed using the six component thermodynamic model of Walshe (1986). This model requires knowledge of the concentrations of major substituting species (SiO_2 , Al_2O_3 , Fe_2O_3 , FeO , MnO , MgO , Na_2O , K_2O , TiO_2 , Cr_2O_3 , CaO) which we have obtained from microprobe analysis.

Calculated temperatures range from 43–347 °C (Table 1). The upper end of the temperature range is consistent with the observed coexistence of chlorite with biotite and/or actinolite and with previous estimates of crystallization temperatures in the inner propylitic zone (e.g., Ballantyne, 1981; Bowman et al., 1987). The lowest temperatures are assumed to be underestimated, probably reflecting a breakdown of the thermodynamic model at low temperatures, but the strong systematic spatial variations suggest that the trend towards lower temperature chlorite crystallization in these samples is real.

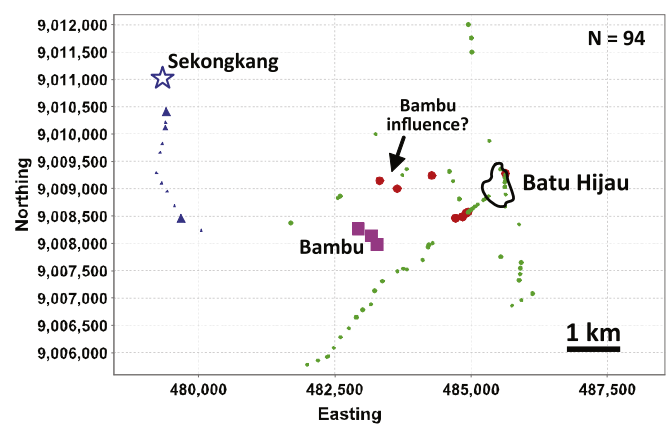
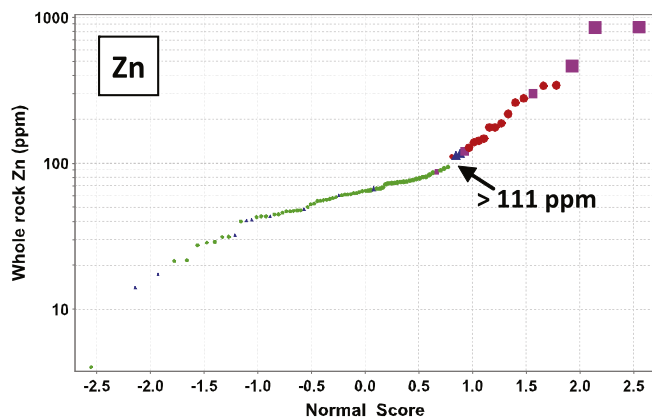
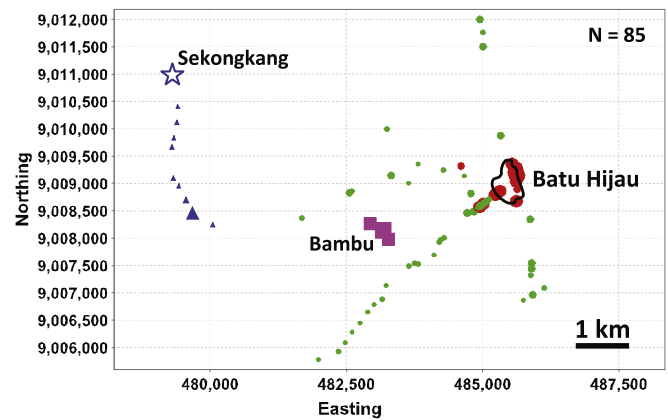
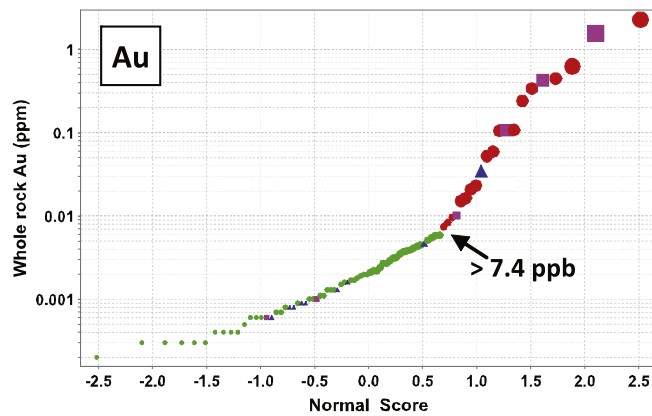
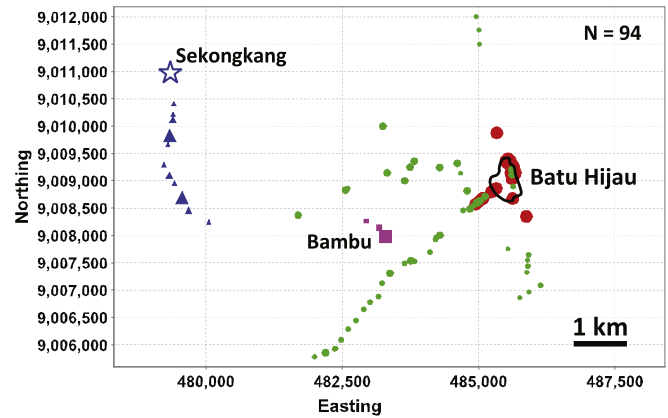
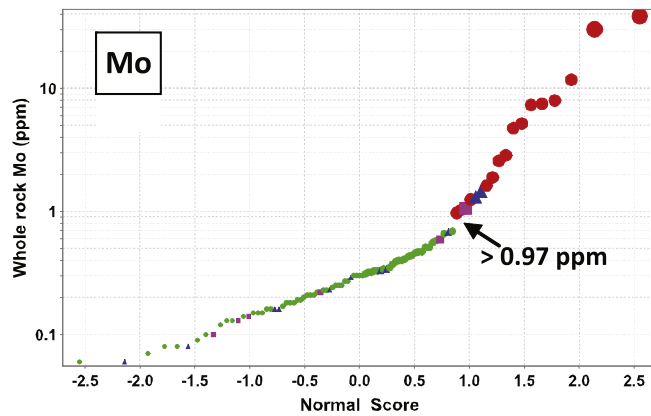
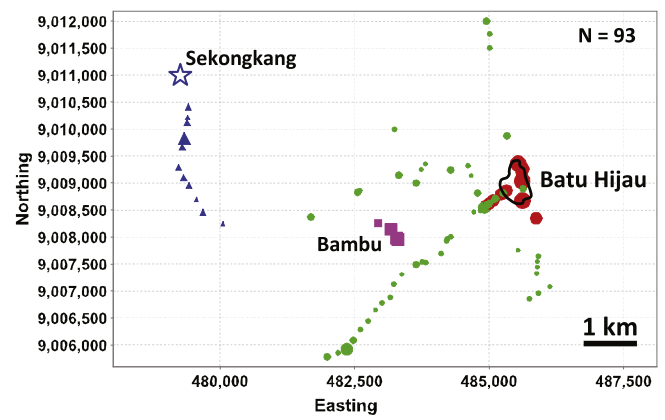
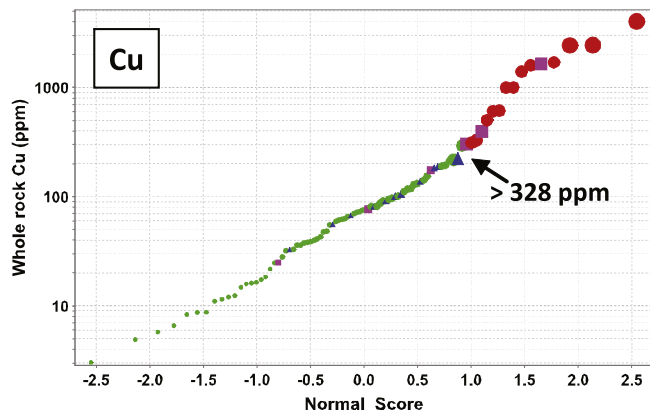
There is a good positive correlation ($r^2 = 0.719$) between chlorite crystallization temperature and radial distance from the Batu Hijau center (excluding Sekongkang, Bambu and proximal tonalite/skarn samples), supporting the inference that these propylitic chlorites formed within the influence of the Batu Hijau hydrothermal system (Fig. 7). As with their trace element compositions, the proximal, tonalite- and skarn-hosted chlorite grains are anomalous, in having lower than

expected calculated crystallization temperatures. The fact that these are observed in pre-, syn- and post-main stage mineralization tonalite and skarn samples implies that they represent a late chlorite-forming event, perhaps reflecting a final thermal collapse of the system that only affected the central ore zone.

In map view, the contoured chlorite thermometry data define a marked thermal high associated with Batu Hijau (Fig. 8) with a WNW–ESE extension that follows the trend of the inner propylitic alteration zone towards Sekongkang (Fig. 2). The steeper thermal gradients to the north, south and southwest of Batu Hijau are readily apparent and can explain the variable trends in trace element concentrations and element ratios in chlorite noted earlier.

5.3. Comparison with whole rock data

In order to provide significant added-value for exploration, mineral chemistry vectors need to define a broader footprint and/or give directional information at greater distances and/or with greater precision than can be obtained from conventional whole rock geochemistry. This was tested by generating probability plots for a range of conventional pathfinder elements in porphyry systems (Cu, Mo, Au and Zn), in the same samples from which the chlorite compositional data were obtained, in order to identify mineralization-related data populations. The whole rock data were then plotted in plan view (Fig. 9) and as a function of radial distance from the deposit center (Fig. 10) and the anomalous populations identified. These plots show that anomalous concentrations of Cu (>328 ppm), Mo (>0.97 ppm) and Au (>7.4 ppb) can be identified in samples up to 1 km from the Batu Hijau center. Concentrations of Zn (>111 ppm) are more variable but there are anomalous concentrations at ~1.0–1.5 km, with rare elevated values extending as far as 2.3 km (Figs. 9, 10). However, these distal samples are only 500 m along strike from the Bambu epithermal veins (Fig. 10) so may have been influenced by this later system.



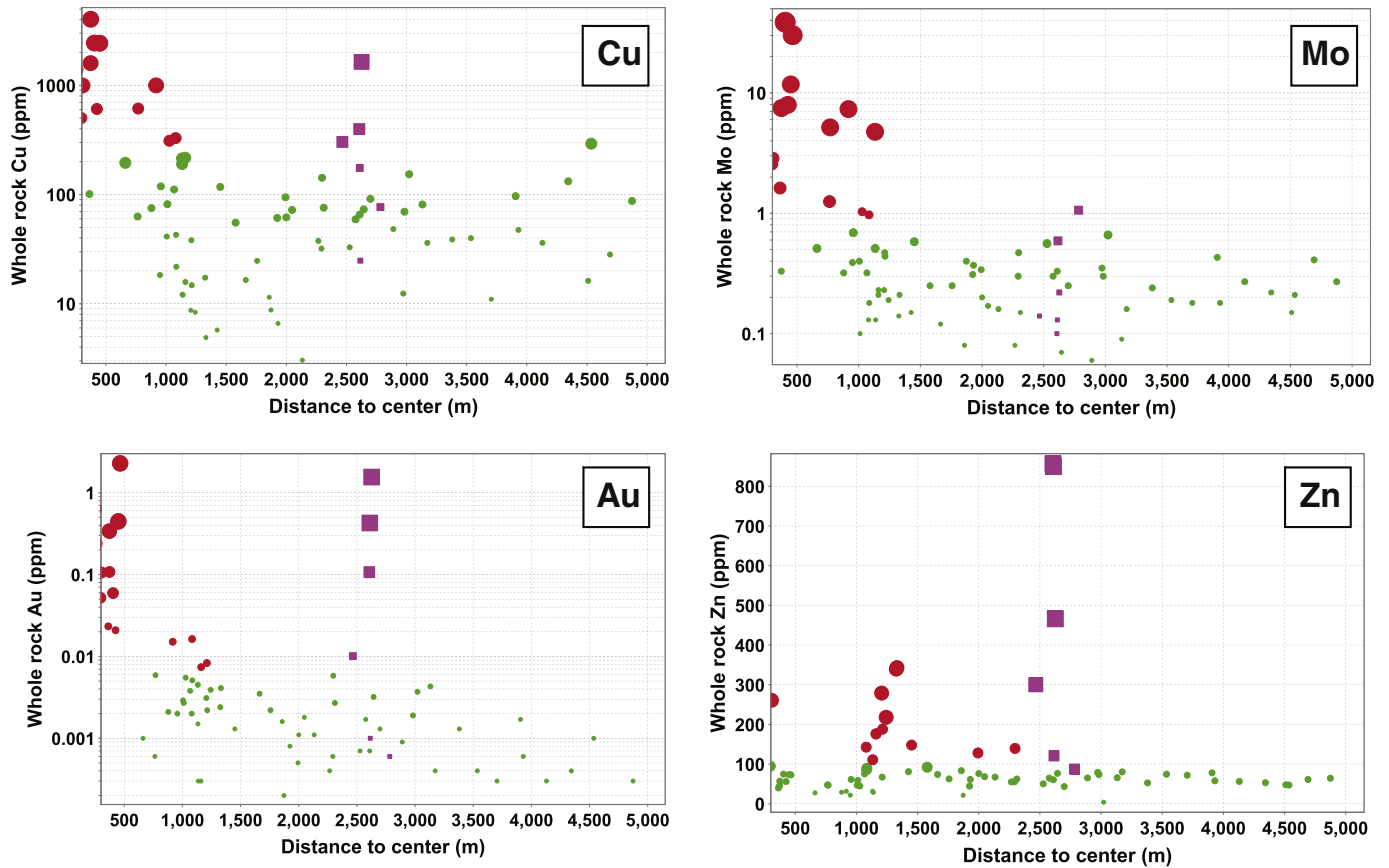


Fig. 10. Plots of concentrations of pathfinder elements (Cu, Mo, Au, Zn) in whole rock as a function of radial distance from the Batu Hijau center. Anomalous populations defined by probability plots (Fig. 9) are shown as red dots; natural background populations are shown as green dots. Data from near the Bambu epithermal veins are highlighted in pink. Symbol sizes are scaled to the concentration value.

Although above-background concentrations of pathfinder elements in whole rock (mostly within 1.0 km) define a footprint consistent with the presence of mineralization in the vicinity, and do broadly increase towards the center, their vectoring potential is limited by significant scatter and lack of distal dispersion (e.g., Fig. 10). Chlorite is effective as a tool at distances beyond about ~800 m (Figs. 5, 6), starting from the outer edge of the whole rock anomalies. It is limited in its proximal applicability because of its disappearance from the higher temperature alteration assemblages where biotite becomes dominant. The trends defined by element ratios in chlorite can be used to indicate the presence of the Batu Hijau center at least 1 km beyond and in some cases more than 3.5 km beyond the distance outlined by conventional whole rock geochemistry. More importantly, chlorite also displays very systematic spatial trends that, conservatively, can be recognized in samples 500 m apart along a traverse orthogonal to the compositional gradient (i.e., towards the system center). Although protolith composition needs to be considered, there is no evidence at Batu Hijau (range in silica content of igneous host rocks from 41 to 69 wt.%), or any of the dozen or so major case studies in the wider AMIRA P765a research project, for a significant protolith effect on the trace elements reported here. Consequently, we conclude that chlorite is a reliable tool for vectoring

towards the hydrothermal center from outside of the whole rock geochemical anomaly associated with porphyry centers.

5.4. The chlorite proximator

The spatial variations in trace element ratios in chlorite can be converted into simple exponential formulae that can be used to predict distance-to-center in porphyry systems such as Batu Hijau. These equations have the form:

$$x = \frac{\ln \left\{ \frac{R}{a} \right\}}{b} \quad (1)$$

where x is the distance in meters, R is the element ratio, and a and b are exponential fit parameters.

A selection of distance prediction equations based on several element ratios, together with their approximate range of validity and correlation coefficients, are given in Table 2. From the relationships discussed above, we conclude that the slope of the exponential relationship will vary according to the form of the thermal anomaly associated with an intrusive system and therefore absolute distance estimates may

Fig. 9. Probability plots and corresponding maps illustrating spatial variations in whole rock composition for four pathfinder elements (Cu, Mo, Au, Zn). Probability plots identify anomalous populations in the datasets (red dots) that are distinguishable from natural background variation (green dots). Symbol sizes are scaled to the concentration value and data from Bambu and Sekongkang are highlighted in pink and blue respectively. Batu Hijau center shown by outline of intense biotite alteration.

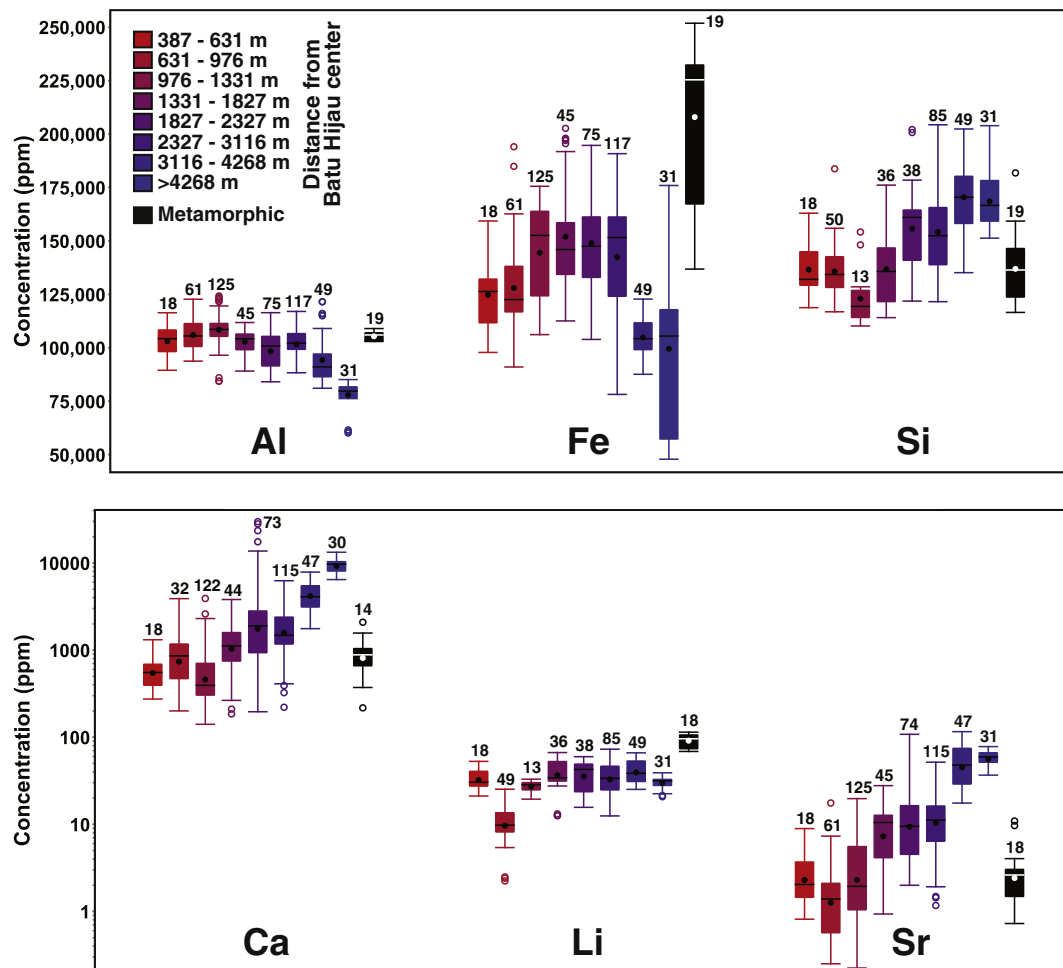


Fig. 11. Comparison of metamorphic chlorite compositions (black symbols) with chlorites from Batu Hijau binned in terms of distance of samples from the porphyry center (warm colors more proximal). Box-and-whisker symbols show: mean value (black dot), median (horizontal line), second and third quartiles (extent of box), whiskers (maximum and minimum values that are not outliers), circles (outliers that are greater than 1.5 times the interquartile range from the box). Numbers of analyses included in each bin are shown.

not be accurate if applied to systems with markedly different thermal gradients to Batu Hijau (or along the western traverse at Batu Hijau). Nonetheless, trends in estimated distances could still be used to vector towards the center of a system, in the same way as the raw element ratios from which the distance estimates were derived.

Applying the Batu Hijau calibrated Ti/Sr proximitor equation to sample-average Ti/Sr data from Batu Hijau itself shows that for 26 out of 28 samples within a 2 km radius of the deposit center, the distance to center is predicted to within ± 170 m. Outside 2 km, where the gradient of the ratio vs. distance relationship starts to decrease, distances to center are underestimated.

5.5. Comparison with metamorphic chlorite

Many terrane hosting porphyry ore deposits include metamorphic host rocks or igneous rocks that have been subjected to relatively low temperature geothermal alteration that is unrelated to porphyry hydrothermal activity. Consequently, the ability to distinguish between porphyry-related propylitic chlorite and that formed in such unrelated systems is desirable.

Batu Hijau chlorite compositions, classified in distance bins relative to the porphyry center, have been compared with metamorphic chlorite

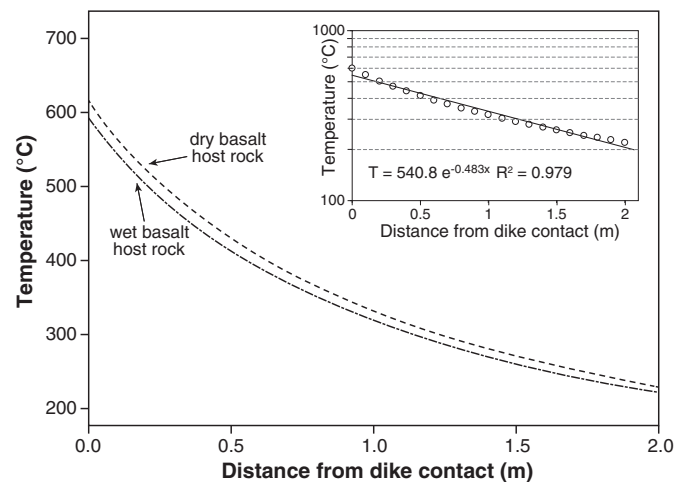


Fig. 12. Numerical model predicting maximum temperature attained due to thermal conduction as a function of distance from a cooling dike for both wet and dry basaltic host rocks (modified after Delaney, 1986). Inset shows model data plotted on a logarithmic temperature axis, with an exponential best-fit line. In the fit equation, T = temperature and x = distance from dike margin.

from two Proterozoic metamorphic terranes in Australia: the Georgetown Inlier in north Queensland and the Entia Dome in the Northern Territory. The Georgetown samples are greenschist facies metabasalts from the Dead Horse Metabasalt unit (Baker et al., 2010). The Entia Dome samples comprise orthogneisses and calc-silicate gneisses from the Entia Gneiss Complex (Wade et al., 2008). Thus, the sample suite covers a range in bulk compositions that span the range studied at Batu Hijau.

The comparison shows that a number of elements distinguish the metamorphic chlorite from the propylitic chlorite, irrespective of the wide range in bulk composition of the metamorphic rocks (Fig. 11). In particular, Fe and Li concentrations are higher in metamorphic chlorite than in most of the Batu Hijau chlorites analyzed. Distal propylitic chlorite is typically depleted in Al, Fe and Li and enriched in Ca, Sr and Si relative to metamorphic chlorite compositions; this distinction is particularly important given that the most critical area in which discrimination would be necessary is in the distal parts of porphyry-related propylitic domains where other indicators of a porphyry system are likely to be lacking. Although less diagnostic, Ti (higher in metamorphic chlorite), and Mg, Zn, Sb, As, Ag, and U (lower in metamorphic chlorite) can also be potentially used as discriminators.

6. Discussion and conclusions

Major ore deposits are increasingly less likely to be discovered at the Earth's surface and exploration is therefore more likely to require probing beneath a kilometer or more of barren or weakly altered cover rocks. Drilling to such depths is extremely costly, so the development of a better understanding of hydrothermal alteration patterns and tools to identify proximity to a mineralized center based on analysis of a limited number of drill core or surface samples are of significant interest.

Here, we show that clear patterns in the trace element chemistry of chlorite are developed in the propylitically altered halo of a large porphyry ore deposit. The observed systematic trace element patterns are most likely due to one or both of the following mechanisms: (1) dispersion outward by migrating hydrothermal fluids, as is clearly documented by the large precious and base metal anomalies that surround such deposits (e.g., Sillitoe, 2010); (2) a thermal control of element substitution in chlorite. In the case of Ti, a high field strength element notable for its limited mobility in igneous or hydrothermal systems, the former mechanism is considered unlikely. However, metals such as Zn and Mn are typically enriched in halos surrounding porphyry deposits and are significantly enriched in chlorite above whole rock concentrations. Therefore, advective transport to the site of Zn–Mn-rich chlorite crystallization would appear to be likely.

In particular, Ti shows a very strong relationship with distance from the hydrothermal center which we argue is primarily a function of crystallization temperature. The approximately exponential decrease in Ti content with distance is consistent with thermal gradients expected around cooling intrusions (e.g., Delaney, 1986; see Fig. 12). We suggest that this exponential relationship breaks down at a certain distance from the center where a transition to “background chlorite” – that did not crystallize in the presence of propylitic hydrothermal fluids – occurs. This distal chlorite appears to show no systematic compositional variation relative to the porphyry center and also displays more scatter in compositional parameters (e.g., Fig. 5).

We are not aware of previous studies documenting the thermal dependence of Ti in chlorite although this control is known for biotite (Henry & Guidotti, 2002; Henry et al., 2005; Patiño Douce, 1993; Patiño Douce et al., 1993). Similar to biotite, we propose that the substitution of Ti into the octahedral site in chlorite is thermally-controlled, requiring coupled substitutions involving multiple cations and possibly anions. Substitution could also account for many of the other systematic trace element patterns that we have recognized that either correlate positively (e.g., Mg, Al, V) or negatively (Li, B, Ca, Sr, Ba) with Ti and temperature. Biotite typically contains much higher concentrations of Ti

than we have determined in chlorite and so the precipitation of Ti-bearing oxides (most commonly titanite, but also rutile at Batu Hijau) is an expected outcome of the biotite → chlorite replacement reaction, the most common chlorite-forming reaction we have observed. The liberation of Ti in this reaction has also been reported from retrograde metamorphic rocks (Eggleton & Banfield, 1985). The limited take-up of Ti by chlorite may be due to the high levels of octahedral Al that typify the chlorite structure (Ryan & Reynolds, 1997). The buffering of the Ti content of chlorite by the excess Ti produced from the biotite breakdown reaction may explain why chlorite incorporates Ti in such a systematic way, possibly in part related to an inverse temperature dependence of Al in the octahedral site.

In addition to temperature, other factors that could control substitution of Ti (and other elements) are the Al, Fe and Mg content of precursor mafic phases which in turn reflect the chemistry of the protolith rocks, the oxidation state and the pH of the fluids concerned (e.g., Shikazono & Kawahata, 1987). Batu Hijau provides a relatively uniform protolith environment in which such factors are limited. The somewhat anomalous chlorite compositions recorded in the tonalite samples could be due to protolith chemistry or may reflect a different origin of chlorite from that developed in the propylitic halo. Such controls of the concentration of Ti (and other trace elements) in chlorite require further investigation in more compositionally heterogeneous systems. By analogy with Ti substitution in biotite (Patiño Douce, 1993), oxidation state may influence Ti in chlorite; however, it will be difficult to evaluate the relative roles of temperature and redox in natural samples from the propylitic environment because of the strong coupling between these two parameters.

Some elements, such as Zn and Mn, are easily accommodated in the chlorite structure (Deer et al., 1966) and may attain significant concentrations. At Batu Hijau, these show a chlorite concentration maximum at a distance of about 1.3 km from the center of the system which mirrors the whole rock anomalies defined by these metals (Fig. 9). This is a characteristic dispersion pattern around porphyry deposits (Sillitoe, 2010). Consequently, these elements are thought likely to be advected by magmatic-hydrothermal fluids to at least this distance from the porphyry deposit itself. It has been previously suggested that hypersaline magmatic brines, known to be enriched in Mn, Zn and Pb (Audétat et al., 2008; Landtwing et al., 2005; Ulrich et al., 1999; Wilkinson et al., 2008), may have precipitated these metals during cooling in contact with rocks undergoing propylitic alteration and dilution with meteoric water (Hemley & Hunt, 1992). Additional elements that show comparable behavior to this are Fe, Co, Eu and, to a lesser extent, Li.

The thermal dependence of Ti substitution in chlorite provides a powerful tool for mineral exploration in the propylitic environment. The recognition that certain monovalent and bivalent trace elements (Li, K, Ca, Ni, Co, Sr, Ba, Pb) tend to increase in chlorite with distance from porphyry centers allows the generation of Ti/x ratios that vary up to four orders of magnitude. If multiple samples are available, these ratios can provide a sensitive indicator of direction towards a heat source and can also be calibrated to enable estimation of distance from an unknown hydrothermal center, even when it is located at depth. Although chlorite geothermometry alone has been shown to identify the thermal anomaly associated with the Batu Hijau deposit, calculated temperatures vary by less than an order of magnitude and display significant scatter so this is a relatively imprecise vectoring tool. In the case of Batu Hijau, chlorite proximator ratios and geothermometry could reduce the exploration area to around 3 km² from an initial target area of at least 40 km² (e.g., Fig. 8).

We have shown that gradients in chlorite compositions can map out the thermal structure of the broader magmatic system to which an individual mineralized porphyry intrusion relates. This opens up the possibility that the tool can be combined with conventional gravity or magnetic data in order to prioritize geophysical targets that are also thermal anomalies. Significantly, this should work even when an

intrusion is blind to surface as long as its propylitic envelope is preserved and can be sampled.

Although this method can potentially provide a powerful way to identify the centers of hydrothermal systems from within propylitic altered domains, the results presented have not yet been fully interrogated in terms of the potential fertility (i.e., extent of mineralization) of a system. Comparison between a number of porphyry deposits studied in the AMIRA P765A project suggests that the variability of Zn and Mn concentration maxima in chlorite is related to metal endowment, perhaps reflecting the total mass of these metals fluxed through the system. Work is ongoing to establish whether these, and other, criteria can be used as a consistent indicator of porphyry system fertility.

7. Funding source

This work was carried out as part of AMIRA International project P765A, funded by a consortium of 18 mining companies. Project aims and objectives were agreed with sponsors at the start of the project and refined during the course of the research at 6-monthly review meetings. Samples were collected by members of the project team and geological staff from PT Newmont Nusa Tenggara. All analytical data were collected, processed and interpreted, and the article written, by the authors. The paper was submitted for publication following expiry of the non-use confidentiality period.

Acknowledgments

This work was conducted as part of AMIRA International research project P765A. We thank Alan Goode, Peter Camburn and Adele Seymon at AMIRA and all the industry sponsors of P765A for their generous sponsorship of this research. We are extremely grateful to Newmont for access to the deposit and the geologists on site at Batu Hijau for logistical support and help with sample collection. The University of Tasmania (AMIRA P765A) provided financial assistance and Lakehead University and Imperial College London contributed in-kind support. We would like to acknowledge the valuable contributions of the entire P765A project team, Karsten Goemann in the Central Science Laboratories at the University of Tasmania for assistance with microprobe analyses, and Paul Agnew (Rio Tinto Exploration) for his unwavering support of this work and ongoing studies.

References

- Adams, C.G., 1984. Neogene larger foraminifera, evolutionary and geological events in the context of datum planes. In: Tusch, R., Ikebe, I. (Eds.), *Pacific Neogene Datum Planes*. University of Tokyo Press, Tokyo, pp. 47–68.
- Audétat, A., Pettke, T., Heinrich, C.A., Bodnar, R.J., 2008. The composition of magmatic-hydrothermal fluids in barren and mineralized intrusions. *Econ. Geol.* 103, 877–908.
- Baker, M.J., Crawford, A.J., Withnall, I.W., 2010. Geochemical, Sm–Nd isotopic characteristics and petrogenesis of Paleoproterozoic mafic rocks from the Georgetown Inlier, north Queensland: implications for relationship with the Broken Hill and Mount Isa Eastern Succession. *Precambrian Res.* 177, 39–54.
- Ballantyne, G.H., 1981. *Chemical and Mineralogical Variations in Propylitic Zones Surrounding Porphyry Copper Deposits*. (PhD Thesis), University of Utah (208 pp.).
- Berggren, W.A., Kent, D.V., Swisher, C.C., Aubry, M.-P., 1995. A revised Cenozoic geochronology and chronostratigraphy. In: Berggren, W.A., Kent, D.V., Aubry, M.-P., Hardenbol, J. (Eds.), *Geochronology, Time Scales and Stratigraphic Correlation*. SEPM Special Publication No. 54, pp. 129–212.
- Bowman, J.R., Parry, W.T., Kropp, W.P., Kruer, S.A., 1987. Chemical and isotopic evolution of hydrothermal solutions at Bingham, Utah. *Econ. Geol.* 82, 395–428.
- Cooke, D.R., Hollings, P., Wilkinson, J.J., Tosdal, R.M., 2014. *Geochemistry of porphyry deposits*. In: Holland, H.D., Turekian, K.K. (Eds.), *Second edition Treatise on Geochemistry* 13. Elsevier, Oxford, pp. 357–381.
- Deer, W.A., Howie, R.A., Zussman, J., 1966. *An Introduction to the Rock Forming Minerals*. John Wiley and Sons, New York (528 pp.).
- Delaney, P.T., 1986. Conductive cooling of dikes with temperature-dependent thermal properties and heat of crystallization. USGS Open File Report, 86–444 (69 pp.).
- Dilles, J.H., Solomon, G.C., Taylor, H.P., Einaudi, M.T., 1992. Oxygen and hydrogen isotope characteristics of hydrothermal alteration at the Ann-Mason porphyry copper deposit, Yerington, Nevada. *Econ. Geol.* 87, 44–63.
- Eggleston, R.A., Banfield, J.E., 1985. The alteration of granitic biotite to chlorite. *Am. Mineral.* 70, 902–910.
- Garwin, S., 2000. *The Setting, Geometry & Timing of Intrusion-Related Hydrothermal Systems in the Vicinity of the Batu Hijau Copper–Gold Deposit, Sumbawa, Indonesia*. (PhD Thesis). University of Western Australia.
- Garwin, S., 2002. The geological setting of intrusion-related hydrothermal systems near the Batu Hijau porphyry copper–gold deposit, Sumbawa, Indonesia. *Society of Economic Geologists, Special Publication No. 9* pp. 333–366.
- Gustafson, D.L., Hunt, J.P., 1975. The porphyry copper deposit at El Salvador, Chile. *Econ. Geol.* 70, 857–912.
- Hamilton, W., 1979. *Tectonics of the Indonesian region*. U.S. Geological Survey Professional Paper v. 1078 (345 pp.).
- Hemley, J.J., Hunt, J.P., 1992. Hydrothermal ore-forming processes in the light of studies in rock-buffered systems: II. Some general geologic applications. *Econ. Geol.* 87, 23–43.
- Henry, D.J., Guidotti, C.V., 2002. Ti in biotite from metapelitic rocks: temperature effects, crystallochemical controls and petrologic applications. *Am. Mineral.* 87, 375–382.
- Henry, D.J., Guidotti, C.V., Thomson, J.A., 2005. The Ti-saturation surface for low-to-medium pressure metapelitic biotites: implications for geothermometry and Ti-substitution mechanisms. *Am. Mineral.* 90, 316–328.
- Hutchison, C.S., 1989. *Geological evolution of Southeast Asia*. Oxford Monographs on Geology and Geophysics no. 13 (368 pp.).
- Landtwing, M.R., Pettke, T., Halter, W.E., Heinrich, C.A., Redmond, P.B., Einaudi, M.T., Kunze, K., 2005. Copper deposition during quartz dissolution by cooling magmatic-hydrothermal fluids: the Bingham porphyry. *Earth Planet. Sci. Lett.* 235, 229–243.
- Lowell, J.D., Guilbert, J.M., 1970. Lateral and vertical alteration–mineralization zoning in porphyry ore deposits. *Econ. Geol.* 65, 373–408.
- Meinert, L., 1992. Skarns and skarn deposits. *Geosci. Can.* 19, 145–162.
- Norman, D.K., Parry, W.T., Bowman, J.R., 1991. Petrology and geochemistry of propylitic alteration at Southwest Tintic, Utah. *Econ. Geol.* 86, 13–28.
- Patiño Douce, A.E., 1993. Titanium substitution in biotite: an empirical model with applications to thermometry, O_2 and H_2O barometries, and consequences for biotite stability. *Chem. Geol.* 108, 133–162.
- Patiño Douce, A.E., Johnston, A.D., Rice, J.M., 1993. Octahedral excess mixing properties in biotite: a working model with applications to geobarometry and geothermometry. *Am. Mineral.* 78, 113–131.
- Rae, A.J., Cooke, D.R., Phillips, D., Yeats, C., Ryan, C., Hermoso, D., 2003. Spatial and temporal relationships between hydrothermal alteration assemblages at the Palinpinon geothermal field, Philippines: implications for porphyry and epithermal ore deposits. In: Simmons, S.F., Graham, I. (Eds.), *Volcanic, Geothermal, and Ore-forming Fluids: Rulers and Witnesses of Processes within the Earth*. Society of Economic Geologists, Special Publication No. 10, pp. 223–246.
- Ryan, P.C., Reynolds Jr., R.C., 1997. The chemical composition of serpentine/chlorite in the Tuscaloosa Formation, United States Gulf Coast: EDX vs. XRD determinations, implications for mineralogic reactions and the origin of anatase. *Clay Clay Miner.* 45, 339–352.
- Schwartz, G.M., 1947. Hydrothermal alteration in the porphyry copper deposits. *Econ. Geol.* 42, 319–351.
- Seedorff, E., Dilles, J.H., Proffett Jr., J.M., Einaudi, M.T., Zurcher, L., Stavast, W.J.A., Johnson, D.A., Barton, M.D., 2005. *Porphyry deposits: characteristics and origin of hypogene features*. Society of Economic Geologists, Economic Geology 100th Anniversary Volumepp. 251–298.
- Sheppard, S.M.F., Nielsen, R.L., Taylor Jr., H.P., 1971. Hydrogen and oxygen isotope ratios in minerals from porphyry copper deposits. *Econ. Geol.* 66, 515–542.
- Shikazono, N., Kawahata, H., 1987. Compositional differences in chlorite from hydrothermally altered rocks and hydrothermal ore deposits. *Can. Mineral.* 25, 465–474.
- Sillitoe, R.H., 2000. Gold-rich porphyry deposits: descriptive and genetic models and their role in exploration and discovery. *Society of Economic Geologists Reviews* 13, 315–345.
- Sillitoe, R.H., 2010. Porphyry copper systems. *Econ. Geol.* 105, 3–41.
- Simmons, S.F., White, N.C., John, D.A., 2005. *Geological characteristics of epithermal precious and base metal deposits*. Society of Economic Geologists, Economic Geology 100th Anniversary Volumepp. 485–522.
- Soerjaja-Atmadja, R., Maury, R.C., Bellon, H., Pringgoprawiro, H., Polve, M., Priadi, B., 1994. Tertiary magmatic belts in Java. *J. SE Asian Earth Sci.* 9, 13–17.
- Ulrich, T., Günther, D., Heinrich, C.A., 1999. Gold concentrations of magmatic brines and the metal budget of porphyry copper deposits. *Nature* 399, 676–679.
- van Bemmelen, R.W., 1949. *The geology of Indonesia*: Government Printing Office, Martinus Nijhoff, The Hague. Geology 1A, 1–732.
- Wade, B.P., Hand, M., Maidment, D.W., Close, D.F., Scrimgeour, I.R., 2008. Origin of metasedimentary and igneous rocks from the Entia Dome, eastern Arunta region, central Australia: a U–Pb LA-ICPMS, SHRIMP and Sm–Nd isotope study. *Aust. J. Earth Sci.* 55, 703–719.
- Walsh, J.L., 1986. A six-component chlorite solid solution model and the conditions of chlorite formation in hydrothermal and geothermal systems. *Econ. Geol.* 81, 681–703.
- Wilkinson, J.J., Wilkinson, C.C., Vry, V.H., Rusk, B.G., Séguel, J., Zentilli, M., Jeffries, T.E., 2008. *Ore Fluid Chemistry in Super-Giant Porphyry Copper Deposits*: Proceedings of the PACRIM 2008 Congress. Australian Institute of Mining and Metallurgy, Carlton, Victoria, pp. 295–298.